Drug Design, Development and Therapy

Dovepress
Taylor & Francis Group

Open Access Full Text Article

ORIGINAL RESEARCH

Integration of Network Pharmacology, Transcriptomics, and Metabolomics Strategies to Uncover the Mechanism of Chaihuang Qingfu Pill in Treating Sepsis-Induced Liver Injury

Chenbin Zhang[1], Fang Chen[2], Yu Jiang[2], Jun Deng[1], Xiao Yan[1], Xin Yin[1], Bowu Su[1], Wen Liu[1]

[1]Department of Pharmacy, The First Hospital Affiliated with Hunan Normal University (Hunan Provincial People's Hospital), Changsha, 410005, People's Republic of China; [2]Institute of Emergency Medicine, Department of Emergency, Hunan Provincial Key Laboratory of Emergency and Critical Care Metabonomics, Hunan Provincial People's Hospital (The First Affiliated Hospital of Hunan Normal University), Changsha, Hunan, People's Republic of China

Correspondence: Wen Liu, Email liuwen@hunnu.edu.cn

Background: Sepsis is a critical condition triggered by infection and characterized by systemic inflammation and subsequent multiorgan failure. Chaihuang Qingfu Pill (CHQF), an in-hospital formulation developed by Hunan Provincial People's Hospital, is derived from the traditional Chinese medicine compound Qingyi Decoction through optimized herbal compatibility. It possesses pharmacological activities including heat-clearing and purgation, choleretic and anti-jaundice effects, as well as Qi-regulation and mass-resolving properties. Clinically, CHQF is primarily used in the treatment of cholecystitis, pancreatitis, and hepatitis, and has shown potential therapeutic effects in alleviating sepsis-associated liver injury. However, the precise molecular mechanisms and omics-based investigations of CHQF in the context of sepsis remain poorly understood. The NF-κB signaling pathway serves as a central regulatory hub of the inflammatory response. Its activation leads to the excessive expression of pro-inflammatory mediators and cytokines, thereby exacerbating tissue damage and promoting the progression of inflammatory diseases. Consequently, targeting the NF-κB pathway may represent an effective therapeutic strategy for the treatment of sepsis. This study aims to systematically investigate the molecular basis of CHQF in the mitigation of sepsis-associated liver damage.

Purpose: To explore the mechanism of CHQF for the treatment of sepsis-induced liver injury.

Methods: A sepsis mouse model was established via cecal ligation and puncture (CLP). The pharmacological mechanisms of CHQF were explored using network pharmacology, transcriptomics, and metabolomics, which enabled the identification of potential therapeutic targets and pathways, as further validated by in vivo and in vitro experiments.

Results: CHQF administration significantly improved the survival rates, reduced systemic inflammation, and restored liver function in CLP-induced sepsis mice, while also mitigating liver tissue injury. Network pharmacological analysis revealed paeoniflorin, quercetin, hyperforin, and wogonin as the core bioactive compounds of CHQF. Transcriptomic profiling identified key targets, including CD14, CXCL2, CCL2, BIRC5, and CXCL8, and demonstrated a significant downregulation of inflammatory cytokines such as TNF-α, IL-6, IL-1β, IL-17, CCL2, CCL3, CCL4, CXCL2, CXCL3, and CXCL5, alongside NF-κB signaling pathway inhibition. Metabolomic analysis indicated that CHQF treatment reduced the levels of sepsis-related metabolites, including lysophosphatidylcholine (22:6), lysophosphatidylcholine (18:1), 1-LGPC, and C17-sphinganine.

Conclusion: Collectively, these findings suggest that CHQF alleviates sepsis-induced liver injury by modulating the inflammatory response via NF-κB signaling pathway inhibition. This study provides novel insights into the complex molecular mechanisms underlying the therapeutic effects of CHQF in sepsis and enhances the understanding of the pharmacological actions of traditional Chinese medicine in managing sepsis.

Keywords: sepsis, traditional Chinese medicine, liver injury, NF-κB signaling pathway, network pharmacology, multi-omics

Received: 10 March 2025
Accepted: 15 May 2025
Published: 2 June 2025

Graphical Abstract

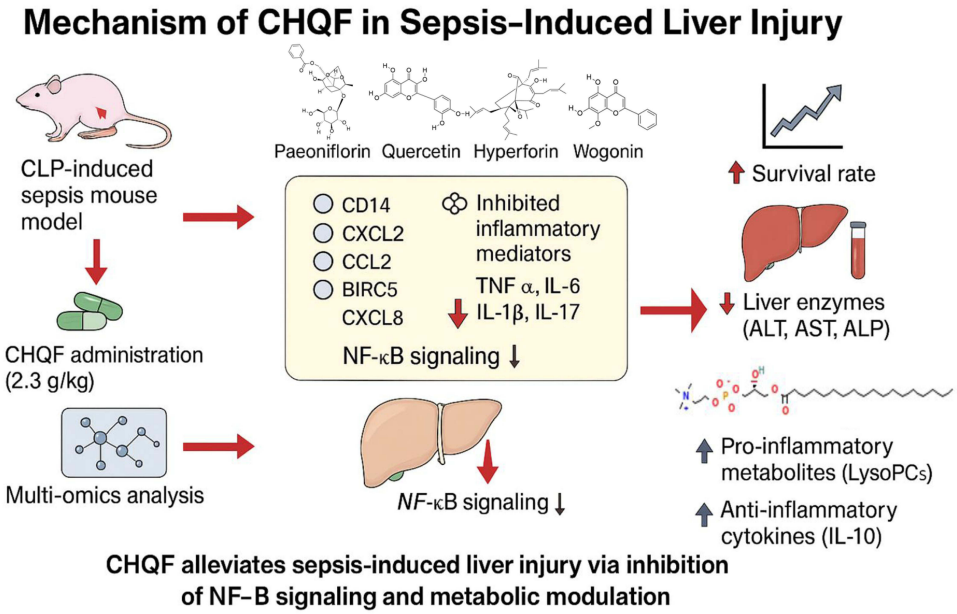

Introduction

Sepsis is a critical syndrome marked by organ dysfunction caused by infection, frequently resulting from conditions such as severe trauma, burns, shock, or major surgery. This condition is commonly linked to systemic inflammatory dysregulation, multi-organ failure, and coagulation disturbances. Sepsis affects an estimated 49 million individuals worldwide each year, leading to approximately 11 million deaths. The World Health Organization has recognized sepsis as a critical global health priority.[1] In China, sepsis represents approximately 20% of the intensive care unit admissions, with a 90-day mortality rate of 35.5%.[2] Sepsis-related mortality has been partly attributed to cytokine storms from early immune hyperactivation.[3] However, despite >30 years of research, sepsis treatment remains largely supportive and antibiotic-based, with no definitive approach for improved patient outcomes. Excessive inflammation during sepsis progression may exacerbate immunosuppression by inducing immune cell apoptosis. Macrophage-mediated inflammation inhibition and apoptosis reduction mitigate the organ damage and improve the survival rates in sepsis models.[4] Consequently, identifying effective therapeutic agents that can alleviate sepsis-induced immunosuppression is critical for enhancing patient survival and outcomes.

Chaihuang Qingfu pill (CHQF), composed of Chaihu (Radix Bupleuri), Huangqin (Scutellariae Radix), Dahuang (Radix Rhei Et Rhizome), Huhuanglian (Picrorhizae Rhizoma), Baixianpi (Dictamni Cortex), Muxiang (Aucklandiae Radix), Jinyinhua (Lonicerae Japonicae Flos), Lianqiao (Forsythiae Fructus), weathered sodium sulfate (thenardite), and Baishao (Paeoniae Radix Alba), is traditionally used in Chinese medicine to alleviate heat, purge bowels, resolve jaundice, and disperse stagnation. This formulation, developed and clinically applied based on the Qingyi Decoction, has shown antimicrobial, anti-inflammatory, and choleretic properties and the ability to adjust intestinal microbiota imbalance, protect the gastrointestinal barrier, and reduce intestinal infections.[5] Qingyi Decoction has demonstrated clinical efficacy in treating pancreatitis.[6] Given the significant similarities in symptomatology and clinical management of pancreatitis and sepsis, the therapeutic effects of CHQF in sepsis were investigated. This formulation showed significant efficacy in treating sepsis-induced liver damage. However, research on CHQF remains limited, and its underlying mechanisms are not well understood. Network pharmacology integrates advanced technologies such as omics approaches (eg, genomics, transcriptomics, and metabolomics), high-throughput screening, network modeling, and computational analysis. This multidisciplinary approach facilitates the identification of intricate interactions within

the "drug-gene-target-disease" network, enabling the prediction of pharmacological mechanisms underlying drug action. Corresponding experiments have been conducted to verify and evaluate drug efficacy, mechanisms of action, and adverse reactions, thereby discovering efficient and low-toxicity drugs.[7]

Metabolomics, an advanced technological method in systems biology, identifies metabolic features that encompass all biochemical changes in biological systems, providing a novel perspective for understanding diseases and drug action. Currently, metabolomics is primarily used to identify biomarkers and metabolic indicators in drug development and clinical toxicology, particularly for studying the systemic impact of toxins on metabolic responses and associated pathogenic mechanisms.[8] Recent metabolomic applications in research on sepsis and liver function damage offers robust directions for diagnosing and treating sepsis-induced liver injury.[9] Transcriptomics studies all the genes expressed by a specific organism or cell at a particular moment. It reveals the comprehensive landscape and variations in gene expression by analyzing RNA expression during the transcription processes. In sepsis-induced liver injury research, transcriptomics is extensively used to elucidate pathogenic mechanisms and disease progression.[10] By analyzing transcriptomic data from patients with sepsis, researchers can identify critical gene expression changes associated with pathological processes, uncovering the molecular mechanisms of biological processes, such as inflammation, oxidative stress, and cell apoptosis.[11] Recent advancements in transcriptomic technologies have enabled a detailed investigation of liver injury in sepsis, including the identification of key signaling pathways that influence inflammation and cell survival.[12] These investigations facilitate the realization of personalized medicine and offer new strategies and approaches for treating sepsis and its complications.[13]

Sepsis progression is complex, with severe cases often exhibiting notable liver damage characterized by hepatocyte mitochondrial swelling, structural damage, and functional abnormalities.[14] Injured hepatocytes can initiate intensified local and systemic inflammatory cascades, further aggravating hepatic dysfunction and affecting the homeostasis of other organs.[15] The nuclear factor kappa B (NF-κB) signaling axis, a key inflammation regulator, activates the expression of pro-inflammatory mediators and cytokines, thereby driving tissue injury and the pathogenesis of various inflammatory conditions.[16] Modulating the NF-κB pathway may represent a potential therapeutic strategy against sepsis. This study, for the first time, employs multi-omics techniques to explore the effects of CHQF in a murine sepsis model induced by cecal ligation and perforation (CLP), potentially mediated through NF-κB pathway regulation.

Materials and Methods

Preparation of CHQF

CHQF is an in-house formulation from Hunan Provincial People's Hospital (Hunan De Kang Pharmaceutical Co., Ltd., Xiang Preparation No. Z20220657000). Its composition includes: Chaihu (Radix Bupleuri), Huangqin (Scutellariae Radix), Dahuang (Radix Rhei Et Rhizome), Huhuanglian (Picrorhizae Rhizoma), Baixianpi (Dictamni Cortex), Muxiang (Aucklandiae Radix), Jinyinhua (Lonicerae Japonicae Flos), Lianqiao (Forsythiae Fructus), weathered sodium sulfate (thenardite), and Baishao (Paeoniae Radix Alba). The CHQF was dissolved in distilled water.

UPLC-MS/MS Analysis of CHQF Components

The CHQF was finely ground at room temperature, and a 50 mg aliquot was dissolved in 500 μL of a pre-cooled extraction solvent at −40 °C, containing isotopically labeled internal standards (methanol:acetonitrile:water = 2:2:1, v/v/v). The solution was vortexed for 30s, followed by the addition of two small steel balls. The mixture was then homogenized at 35 hz for 4 min and subjected to ultrasonic extraction in an ice-water bath for 5 min, with the procedure repeated three times. Following incubation at −40 °C for 30 min, the mixture was centrifuged at 12,000 rpm for 15 min at 4 °C. The supernatant was carefully collected and allowed to stand at −40 °C for an additional 10 min, followed by another centrifugation to yield the supernatant, which was filtered through a 0.22-μm microporous membrane into a sample vial for subsequent analysis.

Chromatographic separation of the target compounds was conducted using a Vanquish ultra-high-performance liquid chromatography system (Thermo Fisher Scientific), equipped with a Phenomenex Kinetex C18 column (21 mm × 100 mm, 2.6 μm particle size). The mobile phase A was composed of a 0.01% aqueous acetic acid solution, while mobile

phase B consisted of a 1:1 (v/v) mixture of isopropanol and acetonitrile. The sample tray was maintained at 4 °C, and the injection volume was 2 μL.

Mass spectrometric analysis was performed using an Orbitrap Exploris 120 mass spectrometer, operated with the Xcalibur software (version 4.4, Thermo). The instrumental parameters were as follows: sheath gas flow rate of 50 Arb, auxiliary gas flow rate of 15 Arb, capillary temperature set at 320 °C, full MS resolution at 60,000, MS/MS resolution at 15,000, collision energy settings at 20/30/40, and spray voltages of +3.8 kV (positive ionization) and −3.4 kV (negative ionization). Figures 1 and 2 depict the total ion current profiles for CHQF.

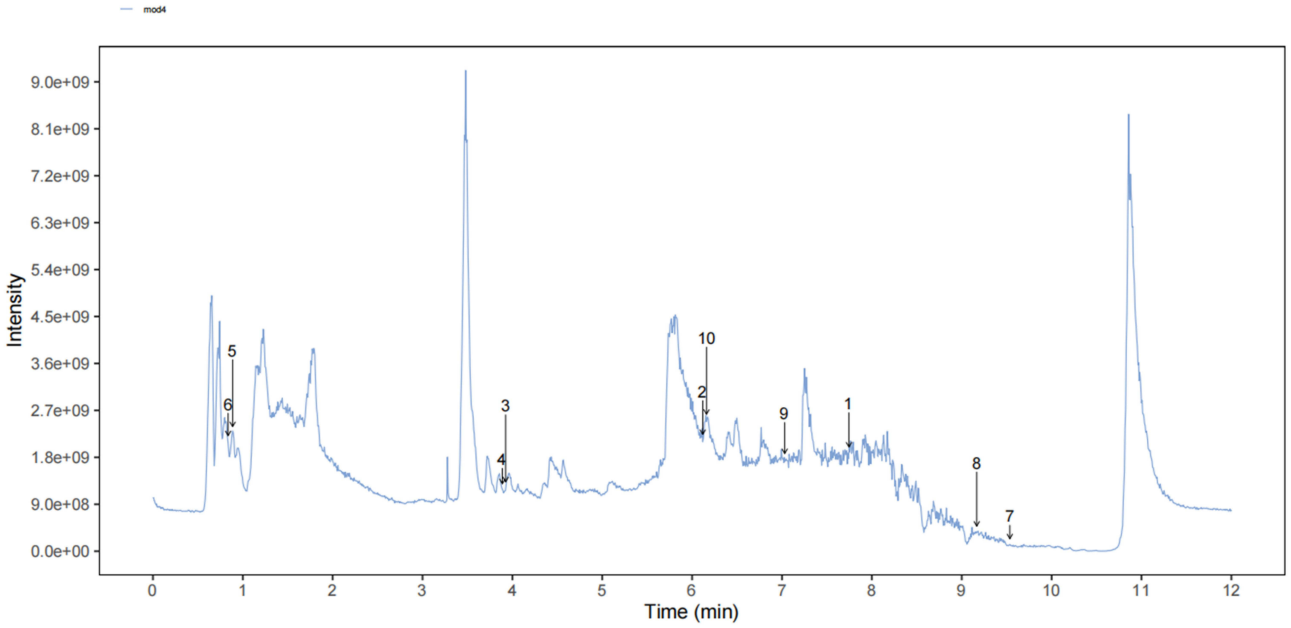

Figure 1 Total ion chromatogram of the CHQF. The peak values represent the top ten ranked compounds (positive ions).

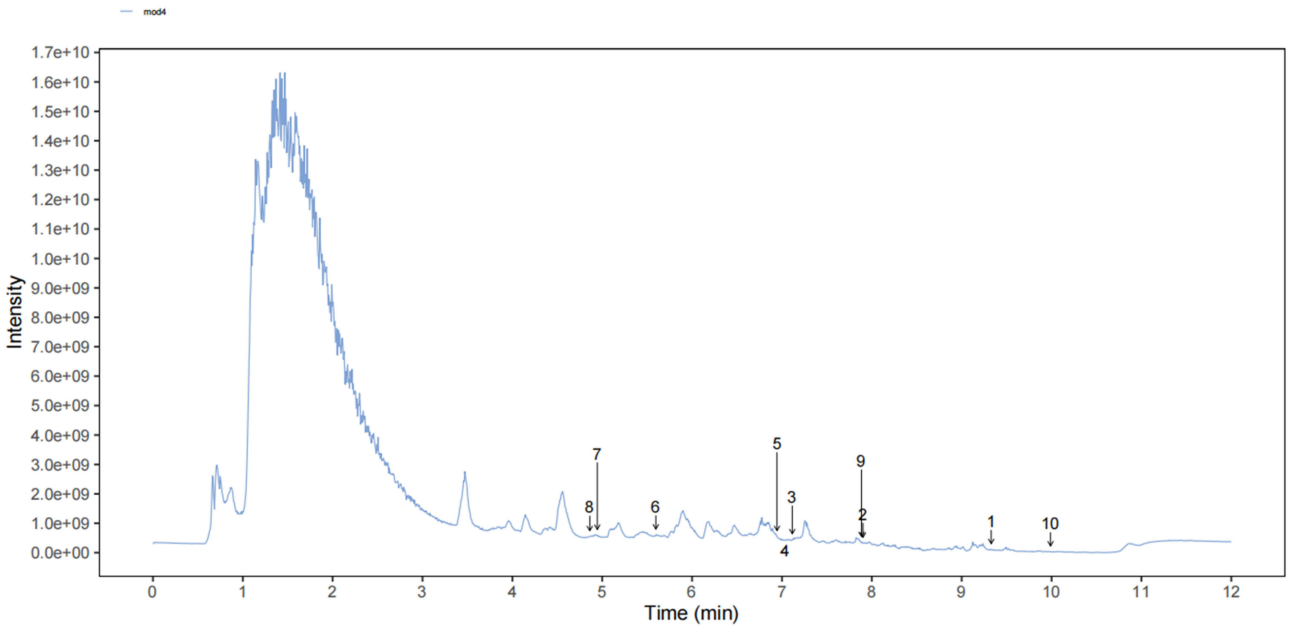

Figure 2 Total ion chromatogram of the CHQF. The peak values represent the top ten ranked compounds (negative ions).

CLP-Induced Sepsis Mouse Model

A total of 60 male BALB/c mice (6–8 weeks old, 20–24 g) were sourced from Hunan SJA Laboratory Animal Co., Ltd. (SCXK(Xiang) 2019–0004). Before the experiments, the mice were acclimated for one week in an SPF-grade facility at the Central Laboratory of Hunan Provincial People's Hospital. Environmental conditions were strictly controlled, maintaining a temperature of 25 ± 2 °C, relative humidity of 60 ± 10%, and a 12-h light/dark cycle. The mice had optionally access to standard pellet diets and sterilized water. Mice were included based on the following criteria: absence of congenital abnormalities, and normal activity levels. Mice displaying signs of pre-existing illness (eg, lethargy, weight loss) or surgical complications (eg, hemorrhage, incomplete ligation) were excluded from the study. All animal experiments were approved by the Animal Ethics Committee of Hunan Provincial People's Hospital (Approval no. LSK2023-117) and conducted in strict accordance with the National Research Council's Guide for the Care and Use of Laboratory Animals (8th edition, 2011) and ARRIVE guidelines 2.0. Every effort was made to minimize animal suffering and reduce the number of animals used.

Abdominal hair removal was performed on mice, which were then randomly assigned to one of three experimental conditions: the sham-operated group, the CLP group, or the CHQF treatment group. The CHQF group was orally administered Chaihuang Qingfu Pill by gavage at the optimal dosage established in previous studies, 2.3 g/kg/day (0.2 mL per dose), for seven consecutive days prior to surgery.[17] This dosage was derived from the clinical human dose using the standard body surface area (BSA) normalization method to ensure translational relevance. The sham and CLP groups were administered with equivalent saline volumes. Sepsis was induced in CLP and CHQF groups via CLP. Mice were anesthetized with isoflurane, and a median abdominal incision, measuring approximately 1–2 cm in length, was performed. The cecum and associated mesentery were exteriorized, followed by ligation of the cecal terminus using 4–0 silk sutures at 1 cm from the distal tip. The cecum underwent double puncture with a 21 G needle, followed by controlled extrusion of minimal fecal content to induce septic insult. The cecum was subsequently repositioned into the abdominal cavity, and the surgical incision was closed in a layered fashion. The sham group underwent laparotomy without CLP, following identical procedural steps. Survival analysis was performed 72 h post-surgery on a random sample of 10 mice from each group. An additional ten mice per group were euthanized 24 h postoperatively to collect the blood, liver, intestine, and intestinal content samples for further analysis.

Histological Analysis

After performing CLP to induce sepsis in mice, liver tissues were collected 24 h post-surgery and fixed in 4% paraformaldehyde. The preserved tissues underwent dehydration, paraffin embedding, and microtome sectioning to produce 4-μm-thick slices. The tissue sections were subjected to hematoxylin and eosin staining, examined, imaged, and scored with an Olympus optical microscope. Hepatic injury was quantitatively assessed using a scoring system:[18] 0 (no injury), 1 (<25%), 2 (25–50%), 3 (51–75%), and 4 (>75%). The criteria for liver injury include hepatocellular degeneration, necrosis, and inflammatory cell infiltration.

Network Pharmacology

The active constituents of CHQF were identified through a combined screening approach based on UPLC-MS/MS analytical results and data retrieved from the Systematic Pharmacology of Traditional Chinese Medicine database (https://www.tcmsp-e.com). The selection of bioactive compounds was guided by criteria of oral bioavailability (OB ≥ 30%) and drug-likeness index (DL ≥ 0.18). Potential sepsis-associated targets were retrieved from GeneCards (https://www.genecards.org/), OMIM (https://omim.org/), TTD (http://db.idrblab.net/ttd/), and DrugBank (https://go.drugbank.com/) databases using "Sepsis" as the query keyword. The Venn R package was employed to generate a Venn diagram and identify intersecting drug-disease targets.

The drug-disease intersecting targets were imported into the Cytoscape 3.8.0 software to create the CHQF-target-disease network, exhibiting the relationship between CHQF and its sepsis targets. The overlapping targets were input into the STRING database (version 12.0) (https://cn.string-db.org/) to construct the protein-protein interaction network, which was subsequently analyzed and visualized using Cytoscape 3.8.0 to identify core targets. Network topology parameters

(Closeness, Betweenness, and Degree) of these targets were obtained using the NetworkAnalyst tool in CytoNCA. CytoNCA was utilized to perform topological parameter analysis for the identification and filtration of core targets.

Functional enrichment analyses, including Gene Ontology (GO) and Kyoto Encyclopedia of Genes and Genomes (KEGG), were performed on the 98 targets using the clusterProfiler, org.Hs.eg.db, enrichplot, pathview, and ggplot2 R packages. GO enrichment analysis was conducted across three domains: biological processes (BP), molecular functions (MF), and cellular components (CC). KEGG signaling pathway enrichment and GO analyses were conducted using R×64 4.0.2 Bioconductor software integrated with the bioinformatics database (https://bioconductor.org/). The intersection of drug-associated and disease-associated gene enrichment was identified based on a significance threshold of $P < 0.05$.

Immunohistochemical Staining

Formalin-fixed, paraffin-embedded 4-μm liver tissue sections were deparaffinized and rehydrated. Antigen retrieval was conducted using 1×citrate buffer solution (pH 6.0, 10007108, Sinopharm Chemical Reagent Co., Ltd). under high-temperature and high-pressure conditions. The sections were blocked with 10% goat serum (PN0038, Wuhan Pinuofei Biological Technology Co., Ltd)., followed by antibody incubation. After incubation, the sections were washed with PBST. For immunohistochemical staining, a diaminobenzidine working solution was applied to the tissues. Finally, the tissue sections were mounted onto slides and analyzed microscopically. Primary antibodies used for immunohistochemical staining were Interleukin-6 (IL-6) (1:300, GB11117, Servicebio), TNF-α (1:200, bs-10802R, Bioss), and CCL2 (1:200, GB11199, Servicebio).

Enzyme-Linked Immune-Sorbent Assay

Triplicate serum sample sets were collected and analyzed using enzyme-linked immunosorbent assay kits (Thermo Fisher Scientific) following the manufacturer's protocol to quantify biomarker levels, including ALP, ALT, AST, IL-2, IL-4, IL-6, IL-10, IL-17A, TNF-α, and IFN-γ. Antibodies were immobilized on a microplate at 4 °C overnight under sealed conditions and subsequently washed with a PBS buffer. Each well was then filled with 300 μL of the PBS buffer and incubated for 1 h for blocking. Blank, standard, and sample wells were subsequently prepared and incubated at 26 °C with plate sealers for 1 h, followed by washing. The stop solution was added to terminate the reaction, and absorbance was recorded at 450 nm using a microplate reader.

Real-Time Polymerase Chain Reaction

Total RNA was isolated from mouse liver tissues using the SteadyPure RNA Extraction Kit (AG21024, Accurate Biotechnology Co., Ltd) following the manufacturer's protocol. cDNA synthesis was performed with the EVO M-MLV RT Mix Kit, utilizing gDNA removal for subsequent quantitative PCR (qPCR) analysis. Additionally, mRNA levels were detected using TB Green Mix for qPCR. PCR amplification was conducted for 40 cycles using a StepOne system with the following conditions: 95 °C for 30s, 95 °C for 5 s, and 60 °C for 34s. mRNA expression levels were quantified relative to GAPDH using the comparative CT method. GAPDH was employed as the internal control and amplified under identical PCR conditions. Table 1 provides the primer sequences.

RNA Sequencing

Liver tissues were collected from Sham, CLP, and CLP+CHQF groups (n=6 per group), immediately ground in liquid nitrogen, and transferred into pre-chilled 1.5 mL centrifuge tubes. Total RNA was extracted using 1 mL TRIzol reagent according to the manufacturer's protocol. After homogenization and incubation at room temperature for 5 min, samples were centrifuged at 13,000 g for 5 min at 4°C. The supernatant was mixed with 200 μL of pre-chilled chloroform, vigorously shaken, incubated at room temperature for 5 min, and centrifuged at 13,000 g for 15 min. The aqueous phase was transferred to a new tube, and an equal volume of isopropanol was added to precipitate RNA. After centrifugation at 13000 g for 10 min at 4°C, the pellet was washed with 75% ethanol, centrifuged at 12000 g for 5 min, air-dried, and dissolved in 20–50 μL of 0.1% DEPC-treated water. RNA samples were stored at –80°C until further analysis.

Table 1 Primer Sequences

Primier Name	Primer Sequence (5'to3')	
	Forward Primer	**Reverse Primer**
IL7	TTCCTCCACTGATCCTTGTTCT	AGCAGCTTCCTTTGTATCATCAC
TNFα	CTCTGTGAAGGGAATGGGTG	GGGCTCTGAGGAGTAGACGATAAAG
IL6	TAGTCCTTCCTACCCCAATTTCC	TTGGTCCTTAGCCACTCCTTC
TNFAIP3	TGTGGGGTGTTCAGGATACTG	GTTCCGAGTGTCTGTCTCCTTA
BIRC3	TTTGAATCCAGCCAACAGTCTG	TGATTTGCTCGGAAGTTCACAG
BIRC2	GCTGGCTTCTATTACATAGGGC	CTCAATCGAGCAGAGTGTGTC
GADD45A	CTGCTGCTACTGGAGAACGAC	CGACTTTCCCGGCAAAAACAAA
CD14	CTCTGTCCTTAAAGCGGCTTAC	GTTGCGGAGGTTCAAGATGTT
CXCL2	TCCAAAAGATACTGAACAAAGGC	TTTGGTTCTTCCGTTGAGGG
CXCL12	TGCATCAGTGACGGTAAACCA	TTCTTCAGCCGTGCAACAATC
CCL2	TTAAAAACCTGGATCGGAACCAA	GCATTAGCTTCAGATTTACGGGT
GAPDH	AGGTCGGTGTGAACGGATTTG	GGGGTCGTTGATGGCAACA

RNA concentration and purity were assessed using a NanoDrop 2000 spectrophotometer, and integrity was confirmed by agarose gel electrophoresis and RIN value determined using the Agilent 5300 system. Poly(A)+ mRNA was enriched using Oligo(dT) magnetic beads. Fragmented mRNA was reverse-transcribed to synthesize the first-strand cDNA using random primers and reverse transcriptase, followed by second-strand synthesis to generate double-stranded cDNA. After end-repair, A-tailing, and adapter ligation, the cDNA fragments were size-selected and amplified by PCR to construct sequencing libraries. Libraries were quantified using Qubit 4.0 and sequenced on the Illumina NovaSeq Xplus platform.

Raw reads were preprocessed using fastp (https://github.com/OpenGene/fastp) to remove adapter sequences and low-quality reads. Reads with >10% N bases or <20 bp in length were discarded. Clean reads were aligned to the reference genome using HiSat2 (http://ccb.jhu.edu/software/hisat2/index.shtml). Mapping quality was assessed based on saturation analysis, gene coverage, and distribution across genomic regions and chromosomes. Gene and transcript expression levels were quantified using RSEM. Differentially expressed genes (DEGs) were identified using DEGseq with thresholds of FDR < 0.05 and $|\log_2 FC| \geq 1$. GO enrichment analysis was performed using Goatools with significance evaluated by Fisher's exact test. To control for false positives, multiple testing corrections were applied using Bonferroni, Holm, Sidak, and FDR methods, and GO terms with adjusted $p \leq 0.05$ were considered significantly enriched. KEGG pathway enrichment analysis was conducted using the KOBAS platform, with enrichment significance also corrected using the Benjamini-Hochberg (FDR) method.

Metabolomic Analyses

Liver samples (30 mg) were collected from sham, CLP, and CLP+CHQF groups of mice. Each sample was transferred into a 1.5 mL Eppendorf tube, supplemented with 20 μL of internal standard solution (0.3 mg/mL L-2-chlorophenylalanine in methanol) and 400 μL of methanol-water mixture (4:1, v/v), along with two pre-cooled stainless-steel beads. Samples were homogenized at low temperature (2 min, 60 hz), followed by ultrasonic extraction in an ice-water bath for 10 min and storage at −20 °C for 30 min. After centrifugation (13,000 rpm, 10 min, 4°C), 300 μL of the supernatant was transferred to LC-MS vials for analysis. Quality control samples were prepared by pooling equal volumes of extraction solutions from all samples to ensure analytical consistency. Metabolite profiling was performed using an Ultimate 3000 high-performance liquid chromatography system coupled with a Thermo Q-Exactive Orbitrap mass spectrometer. Chromatographic separation employed an ACQUITY UPLC HSS T3 column (100 mm × 2.1 mm, 1.8 μm; Waters, Milford, MA, USA), with a mobile phase comprising 0.1% formic acid in water (A) and methanol (B). Gradient elution was as follows: 0–1.5 min, 5% B; 1.5–3 min, 5–30% B; 3–5 min, 30–60% B; 5–7 min, 60–80% B; 7–12 min, 80–100% B; 12–16 min, 100% B; 16–16.5 min, 100–5% B. The mass spectrometry (MS) analysis utilized an electrospray ionization (ESI) source with an acquisition range of 60–900 Da. MS1 resolution was set to 70,000 and MS2 to 17,500. Ionization parameters included spray voltages of 3500 V (POS) and 3100 V (NEG), a capillary temperature of 320°C, an auxiliary gas heater temperature of 375°C, a sheath gas (N_2) flow rate of 30

Arb, and an auxiliary gas flow rate of 10 Arb. Raw data acquisition and preprocessing were conducted using Xcalibur 4.2 SP1 and XCMS (v1.50.1). Corrected data were analyzed with OSI/SMMS (Dalian Chemical Data Solutions, CAS) for differential metabolite identification using VIP > 1 and P < 0.05. Subsequently, the processed data matrix was imported into MetaboAnalyst 6.0 (https://www.metaboanalyst.ca/) for principal component analysis, orthogonal partial least squares discriminant analysis, and metabolic pathway enrichment analysis.

Western Blotting

Total protein was isolated from murine liver tissues utilizing RIPA lysis buffer supplemented with 1% protease and phosphatase inhibitor cocktails. The protein concentration was determined using a NanoDrop One Microvolume UV-Vis Spectrophotometer (Thermo Fisher Scientific). Proteins were thermally denatured at 100 °C for 3 min, resolved on 10% SDS-PAGE, and electrotransferred onto PVDF membranes. The membranes were blocked with 5% non-fat dry milk in TBS-T for 1.5 h at ambient temperature and incubated overnight at 4 °C with primary antibodies, including NF-κB P65 (65 kDa, 1:1000, 8242S, CST), phospho-NF-κB P65 (65 kDa, 1:1000, 3033S, CST), Toll-like Receptor 4 (100/135 kDa, 1:1000, 14358S, CST), MYD88 (37 kDa, 1:1000, 4370S, CST), and GAPDH (1:5000, PMK142S, Biopm). Following primary antibody incubation, membranes were exposed to horseradish peroxidase-conjugated goat anti-rabbit IgG secondary antibodies (1:5000, L3012, SAB) for 1.5 h at room temperature. Immunoreactive bands were visualized with an enhanced chemiluminescent substrate and documented using the Omega Lum C Gel Imaging System (Bio-Rad). Quantitative analysis of protein band intensities was conducted using the ImageJ software (version 1.54F).

Molecular Docking

Molecular docking analysis between the key bioactive compounds and their target proteins was conducted based on prior computational predictions. The 2D structures of the active compounds were retrieved from the PubChem database (https://pubchem.ncbi.nlm.nih.gov) in Structure Data File format. These structures were then converted to 3D conformations using ChemBio3D software (version 14.0.0.117), followed by energy minimization through molecular mechanics force fields to optimize their spatial orientations. The optimized structures were exported as mol2 files for further analysis. The three-dimensional crystal structures of the target proteins were retrieved from the Protein Data Bank (PDB) (http://www.rcsb.org/) and downloaded in PDB format. The PyMOL (version 2.5.4) software was used to remove small-molecule ligands and water molecules from the protein structures, leaving only the protein receptors. The AutoDockTools software was used to add hydrogen atoms to the protein receptors. The ligands and receptors were saved in pdbqt files for compatibility with AutoDock Vina. Molecular docking simulations were conducted using AutoDock Vina to predict the binding affinities and interactions between ligands and receptors. Data were processed and visualized using PyMOL molecular visualization software.

Statistical Analysis

A priori power analysis was performed using G*Power 3.1.9.7 software. Assuming an effect size of 1.2, a significance level (α) of 0.05, and a desired power (1–β) of 0.8, the minimum required sample size per group was calculated to be 5 animals. All experimental groups met or exceeded this sample size requirement. Besides annotation using analysis software, statistical analysis and graphical representation of the data were performed using the GraphPad Prism 6.0 software. The data are presented as mean ± standard deviation. Statistical comparisons between two groups were performed using an independent two-sample *t*-test, while differences among multiple groups were evaluated using one-way analysis of variance. A P-value ≤ 0.05 was considered statistically significant.

Results

Drug Components of CHQF

High-performance liquid chromatography-mass spectrometry (HPLC-MS) was employed to analyze the components of CHQF, identifying 558 metabolites in the positive ion mode (POS) and 552 metabolites in the negative ion mode (NEG). The ion current profiles, both positive and negative, are illustrated in Figures 1 and 2. Tables 2 and 3 present the top 30 components identified in the CHQF for positive and negative ion currents.

Table 2 Chemical Components of the CHQF (POS Top 30)

Name	Formula	Score	mzmed	rtmed	ppm	Type	Adduct
5-Hydroxyindole-3-acetic acid	C10H9NO3	3.94	174.0543	233.3	3.4	POS	[M-H2O+H]+
Schizandrin A	C24H32O6	3.94	417.2258	464.7	3.2	POS	[M+H]+
2-(3,4-dihydroxyphenyl)-5-hydroxy-6,7,8-trimethoxy-chromen-4-one	C18H16O8	3.94	361.0906	367.1	3.4	POS	[M+H]+
P-Synephrine	C9H13NO2	3.93	150.0908	50.5	3.8	POS	[M-H2O+H]+
7,8-dihydroxy-4-phenyl-chromen-2-one	C15H10O4	3.93	255.0643	369.6	3.4	POS	[M+H]+
Hippuric acid	C9H9NO3	3.93	162.0544	240.8	3.3	POS	[M-H2O+H]+
Ornithine	C5H12N2O2	3.93	133.0966	39.4	4.1	POS	[M+H]+
Pyridoxal (Vitamin B6)	C8H9NO3	3.93	150.0546	100.2	2.3	POS	[M-H2O+H]+
(-)-Catechin	C15H14O6	3.93	291.0852	244.4	3.8	POS	[M+H]+
Stearamide	C18H37NO	3.93	284.2937	572.1	3.9	POS	[M+H]+
Creatine	C4H9N3O2	3.92	132.0762	45.6	4.3	POS	[M+H]+
Proline	C5H9NO2	3.92	116.0701	47.1	4.4	POS	[M+H]+
D-Proline	C5H9NO2	3.92	116.0701	47.1	4.4	POS	[M+H]+
Lysine	C6H14N2O2	3.92	147.1122	39	4	POS	[M+H]+
Caprolactam	C6H11NO	3.92	114.0909	223.3	4.3	POS	[M+H]+
4-Guanidinobutyric acid	C5H11N3O2	3.92	146.0918	48.3	4.1	POS	[M+H]+
Eugenin	C11H10O4	3.92	207.0645	380.6	3.6	POS	[M+H]+
Iristectorin B	C23H24O12	3.92	493.1322	297	3.7	POS	[M+H]+
Saikosaponin A	C42H68O13	3.92	781.4708	420.5	3.2	POS	[M+H]+
Valine	C5H11NO2	3.91	118.0858	48.9	4.2	POS	[M+H]+
Corticosterone	C21H30O4	3.91	347.2205	364.7	3.6	POS	[M+H]+
LPC(16:0)	C24H50NO7P	3.91	496.3376	516.2	4.4	POS	[M+H]+
L-Methionine	C5H11NO2S	3.91	150.0577	52.6	4	POS	[M+H]+
DL-METHIONINE	C5H11NO2S	3.91	150.0577	52.6	4	POS	[M+H]+
Stachydrine	C7H13NO2	3.91	144.1013	46.6	4.1	POS	[M+H]+
Carnitine	C7H15NO3	3.91	162.1118	45.3	4.1	POS	[M+H]+
Gamma-Glutamylphenylalanine	C14H18N2O5	3.91	295.1277	224.2	3.9	POS	[M+H]+
D-Glutamine	C5H10N2O3	3.91	147.0758	45.7	4.1	POS	[M+H]+
[2-hydroxy-1-[hydroxy-(7-methoxy-2-oxo-chromen-6-yl) methyl]-2-methyl-propyl] (Z)-2-methylbut-2-enoate	C20H24O7	3.91	377.158	357.9	3.9	POS	[M+H]+
Iraldeine	C13H20O	3.91	193.158	467.6	3.8	POS	[M+H]+

Table 3 Chemical Components of the CHQF (NEG Top 30)

Name	Formula	Score	mzmed	rtmed	ppm	Type	Adduct
Deoxycholic acid	C24H40O4	3.98	391.2848	474.1	1.5	NEG	[M-H]-
Cis-8,11,14-Eicosatrienoic acid	C20H34O2	3.98	305.2481	559.7	1.4	NEG	[M-H]-
3,5-Dimethoxybenzoic acid	C9H10O4	3.98	181.0505	335.8	0.7	NEG	[M-H]-
Tauroursodeoxycholate (sodium)	C26H45NO6S	3.98	498.2892	416.7	0.6	NEG	[M-H]-
Tauroursodeoxycholic acid	C26H45NO6S	3.98	498.2889	473.1	1.1	NEG	[M-H]-
Scutellarin	C21H18O12	3.98	461.0722	291.7	0.8	NEG	[M-H]-
Purpurin	C14H8O5	3.98	255.0298	421.9	0.4	NEG	[M-H]-
Cis-9-Palmitoleic acid	C16H30O2	3.97	253.2168	548.8	1.8	NEG	[M-H]-
Isoleucine	C6H13NO2	3.97	130.0871	63.4	1.9	NEG	[M-H]-
Hydroxyisocaproic acid	C6H12O3	3.97	131.0712	260.5	1.2	NEG	[M-H]-
2-Hydroxyhexanoic acid	C6H12O3	3.97	131.0712	260.5	1.2	NEG	[M-H]-
Myristic acid	C14H28O2	3.97	227.2013	545.5	1.6	NEG	[M-H]-
Traumatic acid	C12H20O4	3.97	227.1287	386.1	0.8	NEG	[M-H]-
Succinic Acid	C4H6O4	3.97	117.0191	82.3	1.9	NEG	[M-H]-
Hyodeoxycholic acid	C24H40O4	3.97	391.2849	435.6	1.1	NEG	[M-H]-
Cis-11.14-Eicosadienoic acid	C20H36O2	3.97	307.2638	574	1.5	NEG	[M-H]-

(*Continued*)

https://doi.org/10.2147/DDDT.S521626

Table 3 (Continued).

Name	Formula	Score	mzmed	rtmed	ppm	Type	Adduct
Trans-11-Eicosenoic acid	C20H38O2	3.97	309.2794	590.4	1.5	NEG	[M-H]-
14-hydroxy-14-(hydroxymethyl)-5,9-dimethyl-tetracyclo [11.2.1.01,10.04,9] hexadecane-5-carboxylic acid	C20H32O4	3.97	335.2227	396.2	0.2	NEG	[M-H]-
Nonadecanoic acid	C19H38O2	3.97	297.2794	599.3	1.7	NEG	[M-H]-
6,7,4'-Trihydroxyisoflavone	C15H10O5	3.97	269.0455	314.4	0.1	NEG	[M-H]-
Pyrrole-2-carboxylic acid	C5H5NO2	3.97	110.0246	225.7	1.4	NEG	[M-H]-
Glyceraldehyde	C3H6O3	3.96	89.0242	51.7	1.8	NEG	[M-H]-
Dihydroxyacetone	C3H6O3	3.96	89.0242	51.7	1.8	NEG	[M-H]-
Linoleic acid	C18H32O2	3.96	279.2323	553.7	2.2	NEG	[M-H]-
Beta-Muricholic acid	C24H40O5	3.96	407.2798	406.4	1.3	NEG	[M-H]-
Alpha-Linolenic acid	C18H30O2	3.96	277.2167	536.8	2.2	NEG	[M-H]-
Baicalin	C21H18O11	3.96	445.0772	312.1	1	NEG	[M-H]-
Pelargonic acid	C9H18O2	3.96	157.1232	456.3	1	NEG	[M-H]-
Glycocholic acid	C26H43NO6	3.96	464.3012	408.3	1.2	NEG	[M-H]-
Chenodeoxycholic acid	C24H40O4	3.96	391.2848	474.1	1.5	NEG	[M-H]-

CHQF Treatment Improves CLP-Induced Sepsis Liver Injury

To assess the therapeutic potential of CHQF in sepsis, a murine model was employed. The impact of CHQF treatment on the survival rate of septic mice was evaluated. The mortality rate of mice in the CLP group significantly increased at 24 h, whereas that of mice treated with CHQF showed a significant decrease at 24 h (Figure 3A). Mouse serum biochemical indicators were quantified to assess the cytoprotective efficacy of CHQF against septic liver injury. Serum levels of the liver function markers ALT, AST, and ALP were significantly elevated in the CLP group but markedly reduced in the CLP+CHQF group after treatment (Figure 3B–D), suggesting that CHQF alleviates sepsis-induced liver damage. Furthermore, inflammatory cytokine expression in mouse serum was measured to determine the systemic inflammation levels. In the CLP group, levels of IL-2, IL-4, IL-6, IFN-γ, TNF-α, and IL-17A significantly increased, while IL-10 levels significantly decreased (Figure 3E–K). Conversely, in the CLP+CHQF group, these inflammatory factors tended towards normalization, indicating that CHQF effectively improved sepsis-induced immunosuppression. Hematoxylin and eosin staining results demonstrated that in the CLP group, the hepatocytes were swollen, sinusoids were diminished, and mild inflammatory cell infiltration was present. Nuclear alterations, vacuolar degeneration, hepatocellular ballooning, and pronounced inflammatory cell infiltration within the portal tract were detected. However, treatment with CHQF significantly reduced this damage (Figure 3L and M), demonstrating promising therapeutic efficacy in significantly reducing liver tissue damage caused by sepsis.

CHQF Treatment Effectively Suppresses Hepatic Inflammatory Infiltration in Septic Mice

Sepsis is frequently characterized by hyperactivation of the immune system, driving a systemic inflammatory response and cytokine storm—a severe immune reaction that can result in widespread tissue damage and multiorgan dysfunction. Immunohistochemical staining revealed that in CLP-induced lesions (Figure 4), the expression of TNF-α, IL-6, CXCL2, and CCL2 in liver tissues was significantly higher in the CLP group compared to the sham and CLP+CHQF groups, as evidenced by increased staining intensity. This indicated elevated activity of these inflammatory cytokines in the CLP group, while CHQF treatment effectively suppressed their expression. It suggesting its role in inhibiting inflammatory signaling, suppressing the NF-κB P65 pathway, and enhancing antioxidant capacity, thereby effectively ameliorating septic liver injury.

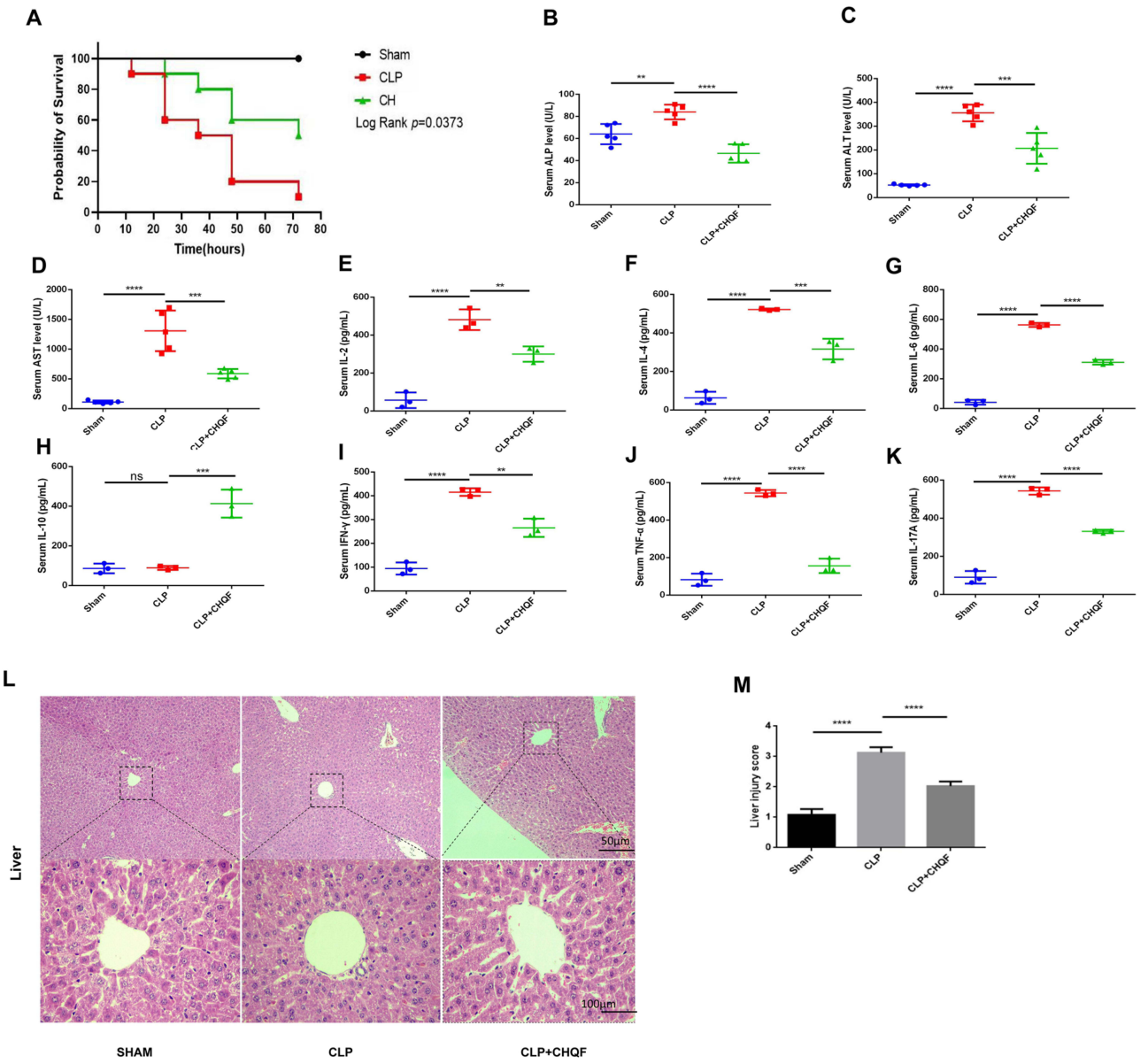

Figure 3 CHQF reduces the mortality rate, hepatic injury, and production of pro-inflammatory cytokines in serum in a mouse model of sepsis. (**A**) Survival curve analysis in a murine sepsis model. Serum levels of (**B**) ALP, (**C**) ALT, (**D**) AST. The levels of (**E**) IL-2, (**F**) IL-4, (**G**) IL-6, (**H**) IL-10, (**I**) IFN-γ, (**J**) TNF-α, (**K**) IL-17A (n=5). (**L**) H&E staining and (**M**) Liver injury score to visualize the histomorphological features and quantitation analysis (n=5). Data are expressed as mean ± SEM. $^{**}P < 0.01$, $^{***}P < 0.001$, $^{****}P < 0.0001$ vs CLP group; ns, not significant.

Network Pharmacology Analysis

From the UPLC-MS/MS analytical results and Systematic Pharmacology of Traditional Chinese Medicine database, 2548 CHQF targets were collected alongside 3196 sepsis targets from the GeneCards database, with 1409 potential targets screened by relevance score ≥ 1.0. Furthermore, 1, 40, and 17 potential sepsis targets were collected from the TTD, OMIM, and DrugBank databases, respectively. Ninety-eight potential curative targets intersected between the CHQF and sepsis targets (Figure 5A). These intersection targets were input into Cytoscape 3.8.0 software to construct an active ingredient-target-disease network comprising 338 nodes and 4468 edges. A total of 98 intersection genes were input into the STRING database, and a protein-protein interaction network was established, consisting of 98 distinct nodes and 1925 interconnecting edges. The cytoNCA plug-in was used to identify the top 16 core genes (Figure 5B and C). The "drug—active compound—target—disease" network was also constructed (Figure 5D). These results indicated that

https://doi.org/10.2147/DDDT.S521626

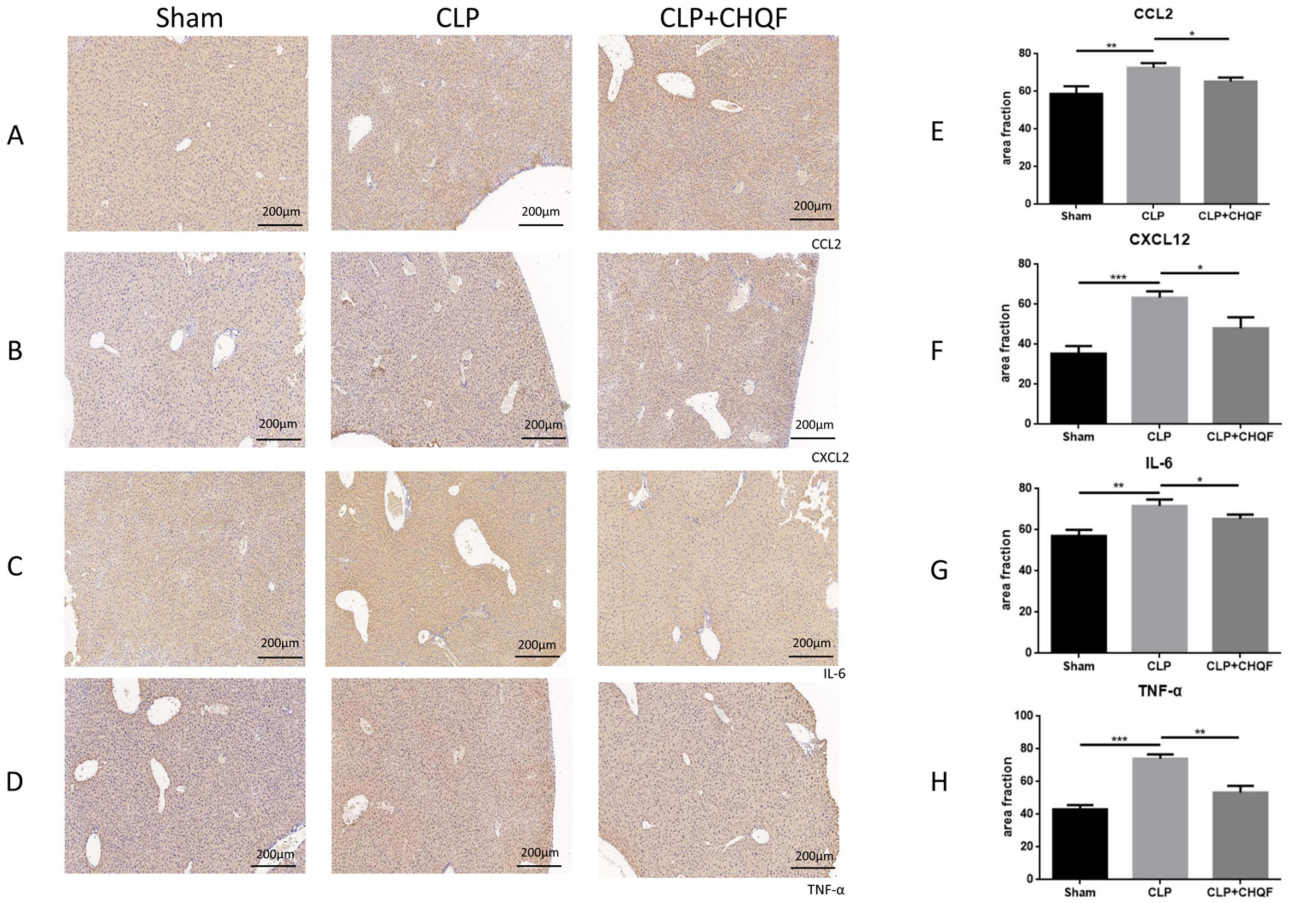

Figure 4 CHQF inflammatory cell infiltration. IHC staining for (**A**) CCL2, (**B**) CXCL2, (**C**) IL-6, (**D**) TNF-α (100×). (**E–H**) Statistical analysis of CCL2, CXCL2, IL-6, TNF-α values. Data presented as mean ± SD(n = 5 /group); **P* < 0.05, ***P* < 0.01, ****P* < 0.001 vs CLP group; ns, not significant.

CHQF treatment for sepsis exhibits multi-component and multi-target effects. In the context of GO enrichment analysis of the intersecting gene targets, CHQF was implicated in modulating cellular responses to lipopolysaccharides, which are molecules of bacterial origin. Additionally, it influenced cellular adaptations to chemical stress, oxidative stress, and reactive oxygen species (Figure 5E). KEGG pathway analysis revealed that CHQF may be involved in modulating the PI3K-AKT, MAPK, IL-17, TNF, and NF-κB signaling pathways (Figure 5F), which are closely linked to inflammatory processes, metabolic regulation, and immune system function,[19] underscoring its potential therapeutic role in sepsis.

Characterization of CHQF-Treated Sepsis via RNA-Seq Analyses

To further characterize the molecular targets of CHQF, transcriptome sequencing was performed on liver tissues from the sham, CLP, and CLP+CHQF groups, yielding an average error rate of 0.0119% with an average Q20 value > 98.17%. Principal component analysis (Figure 6A) revealed distinct clustering of the three groups. The sham group was significantly displaced to the right compared with the CLP and CLP+CHQF groups, whereas the CLP+CHQF group showed a shift towards the sham group relative to the CLP group, indicating a trend toward the recovery of aberrantly expressed genes in the liver tissue post-CHQF administration. Figure 6B and C illustrates the identification of 5911 differentially expressed genes in the CLP group relative to the sham group. Among these, 3119 genes were upregulated and 2792 downregulated. In contrast, the CLP+CHQF group showed 1870 differentially expressed genes, with 986 upregulated and 884 downregulated compared to the CLP group. Figure 6D displays a heatmap of the clustering analysis of NF-κB pathway-related genes, indicating that CHQF effectively downregulated the expression of interleukins,

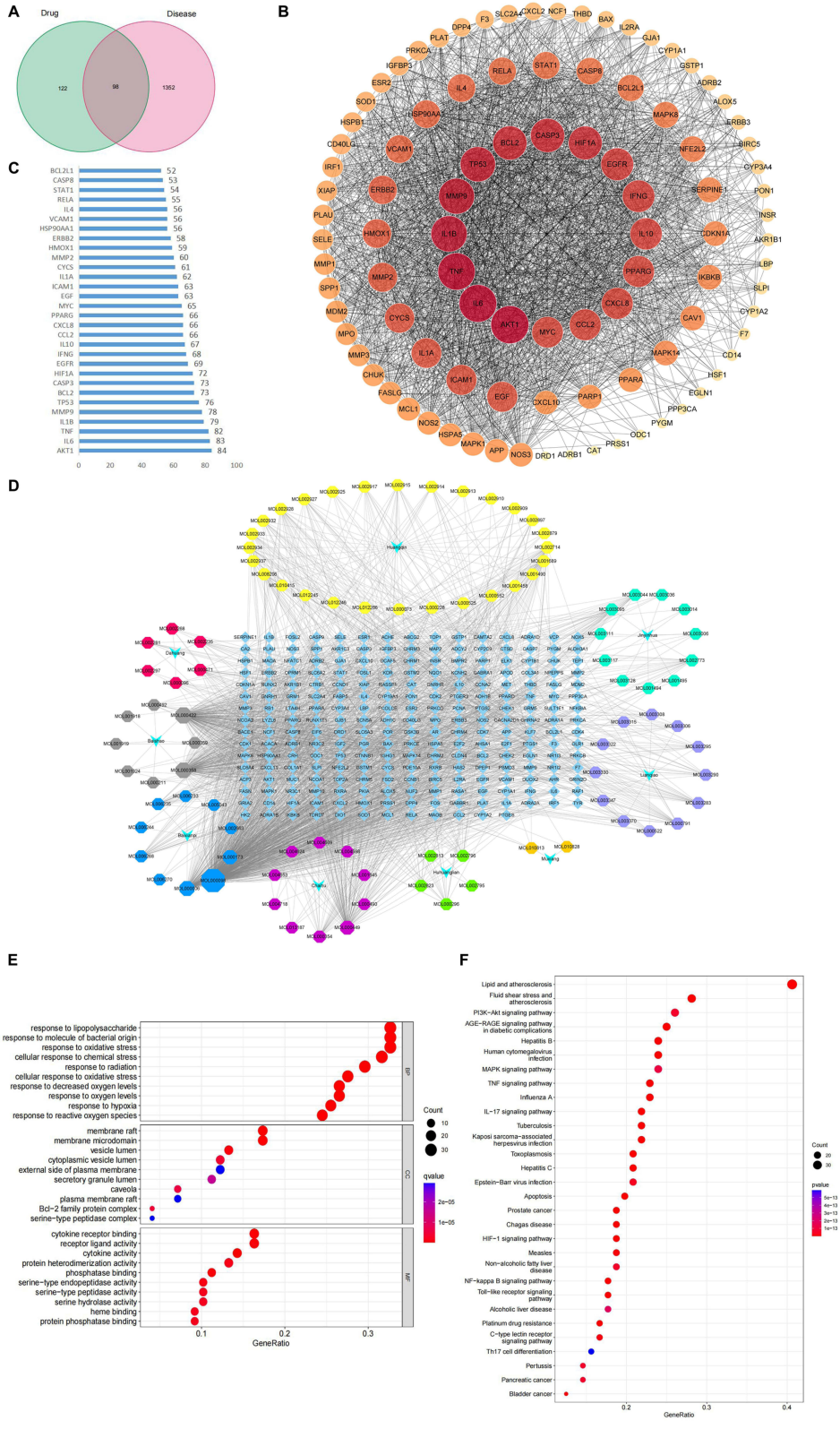

Figure 5 Network Pharmacology uncovers the mechanism of CHQF for sepsis. (**A**) Venn diagram of targets shared by CHQF and sepsis. (**B**) The PPI network of intersection targets. (**C**) Degree of top 30 common targets (number of node-connected edges) of common targets (top 30) in the PPI network. (**D**) Active ingredient−target −disease network diagram. (**E**) GO-enrichment analysis of common targets. (**F**) KEGG pathway analyses of the hub genes.

https://doi.org/10.2147/DDDT.S521626

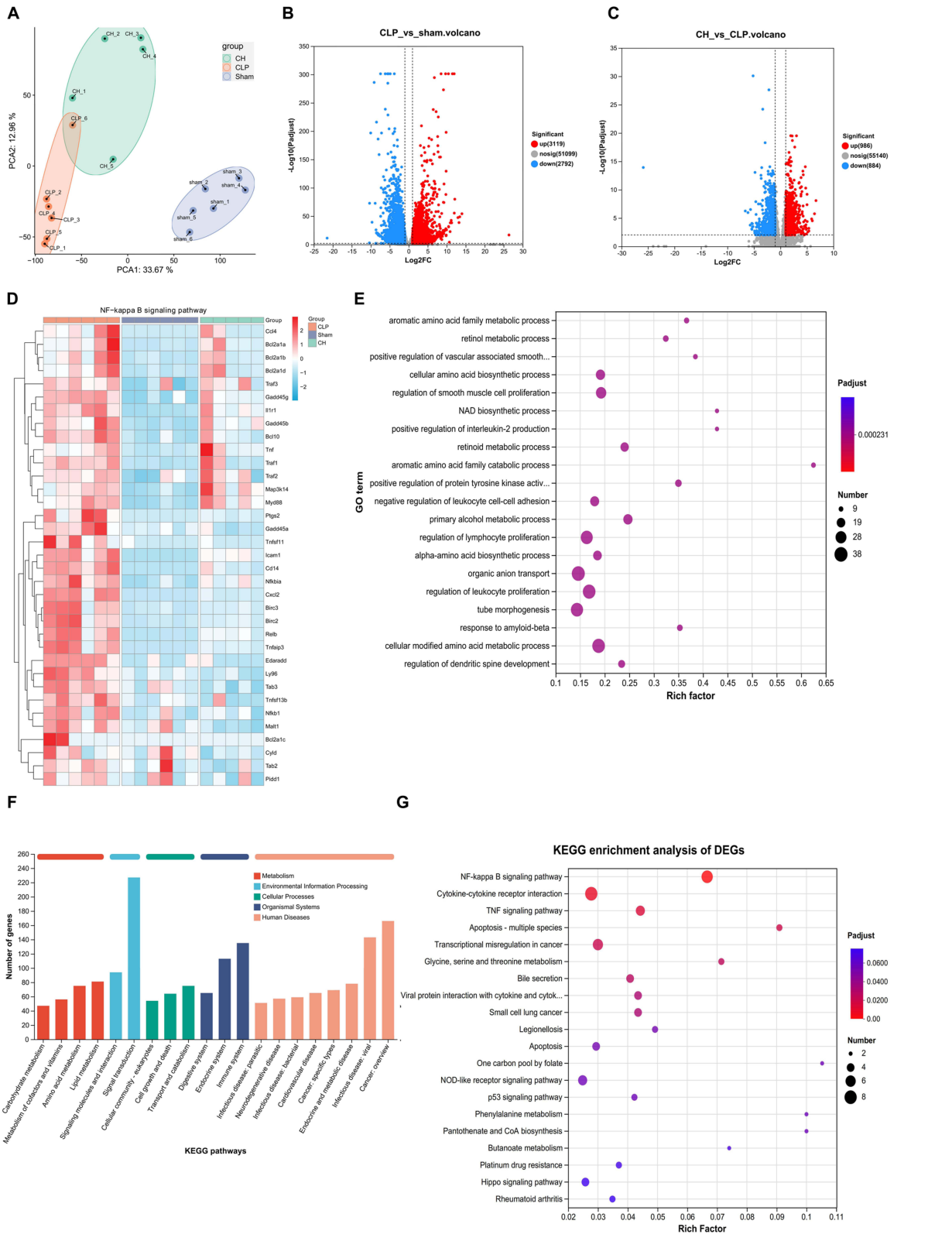

Figure 6 CHQF regulates the expression of genes related to sepsis. (**A**) PCA mapping of Sham, CLP, and CHQF treated samples. (**B**) Volcano plots of upregulated and downregulated DEGs between CLP and Sham groups. (**C**) Volcano plots of upregulated and downregulated DEGs between CHQF and CLP groups. (**D**) Heatmap for hierarchical cluster analysis of DEGs between the samples. (**E**) GO functional enrichment analysis. (**F**) KEGG functional annotation analysis. (**G**) KEGG functional enrichment analysis.(n=6 /group, one data point in the CH group was identified as an outlier and was excluded from the analysis).

chemokines, and TNF-related genes, reducing the inflammatory responses. GO functional enrichment analysis (Figure 6E) revealed that, relative to the CLP group, the differentially expressed genes (DEGs) in the CLP+CHQF group were primarily associated with pathways involved in cellular amino acid catabolism, bile acid and salt transport, and programmed cell death regulation. KEGG functional annotation analysis revealed that in terms of metabolism, genes were mainly enriched in carbohydrates, cofactors and vitamins, and amino acid metabolism. In environmental information processing, genes are primarily enriched in signaling molecules, interactions, and signal transduction. In the context of cellular processes, genes are predominantly linked to transport and catabolic pathways, cell proliferation and apoptosis, as well as the organization and function of the eukaryotic cellular community. Genes in organismal systems are mainly enriched in the immune, endocrine, and digestive systems. In human diseases, genes are predominantly involved in cancer and viral infectious diseases. KEGG gene functional enrichment analysis identified that CHQF primarily affects the NF-κB signaling pathway, TNF signaling pathway, and cytokine-cytokine receptor interaction (Figure 6F and G).

CHQF Reduces the Expression of Inflammatory Cytokines and NF-κB Pathways

The NF-κB signaling pathway plays a pivotal role in mediating inflammatory responses. Integrating preliminary network pharmacology predictions with transcriptomic sequencing analyses, key genes and pathways of significant relevance were identified. CHQF markedly downregulated the TNF-α, IFN-γ, IL-6, CD14, CXCL2, CCL2, TNFAIP3, and GADD45A mRNA expression in the liver tissues of septic mice while increasing the IL-10 mRNA expression level (Figure 7G–Q). Western blot analysis demonstrated a low phosphorylation level of P65 in the liver tissues of the sham group, elevated levels in the CLP group, and significant inhibition by CHQF treatment. Furthermore, the TLR4 and MYD88 protein expression was upregulated in the liver tissues of the CLP group relative to the sham group, whereas CHQF treatment markedly suppressed their expression levels (Figures 7A–F). These results align with the observations from RNA-seq and network pharmacology predictions, indicating that CHQF exerts anti-inflammatory and antioxidant effects through the NF-κB signaling pathway suppression.

Metabolomics Profiling

Metabolomic profiling of mouse liver samples was performed under both negative and positive ionization modes. Principal component analysis was performed to identify differential metabolites among the sham, CLP, CLP+CHQF groups (Figure 8A), indicating a clear separation between these groups. To further elucidate the metabolites contributing to these significant differences, partial least squares discriminant analysis (PLS-DA) was utilized to differentiate the metabolic profiles of the sham vs CLP groups and the CLP vs CLP+CHQF groups (Figures 8B and C). Both comparisons showed good separation and high R2Y and Q2 values, suggesting that CHQF exerted a pronounced modulatory effect on the metabolic landscape of septic mouse liver tissues.

Differential metabolites were screened based on VIP > 1, $P < 0.05$, and fold change thresholds of >2 or <0.5, resulting in 108 differential metabolites. A heatmap was constructed to depict the metabolic alterations across the three experimental groups (Figure 8D). Following CHQF treatment, most metabolites were recovered, indicating a reduction in metabolic disturbances in septic mice. Metabolic pathways were mapped for sham vs CLP and CLP vs CLP+CHQF comparisons (Figure 8E and F). The primary metabolic pathways affected by CHQF in CLP-induced sepsis included taurine and hypotaurine metabolism, pantothenate and CoA biosynthesis, glycerophospholipid metabolism, and riboflavin metabolism (Tables 4 and 5).

Molecular Docking Validation

Based on these findings, four core components (paeoniflorin, quercetin, hyperforin, and wogonin) and five corresponding core targets (CD14, CXCL2, CCL2, BIRC5, and CXCL8) were identified. Molecular docking was conducted to evaluate the binding interactions of these four core components with five core targets, according to the results obtained from network pharmacology and transcriptomics. The binding energy of active molecules to potential targets indicates their binding affinity, with lower values indicating stronger binding interactions.[20] The molecular docking results revealed the following binding energies: paeoniflorin-CD14 (−6.9 kcal/mol), quercetin-CXCL2 (−7.8 kcal/mol), quercetin-CCL2

 https://doi.org/10.2147/DDDT.S521626

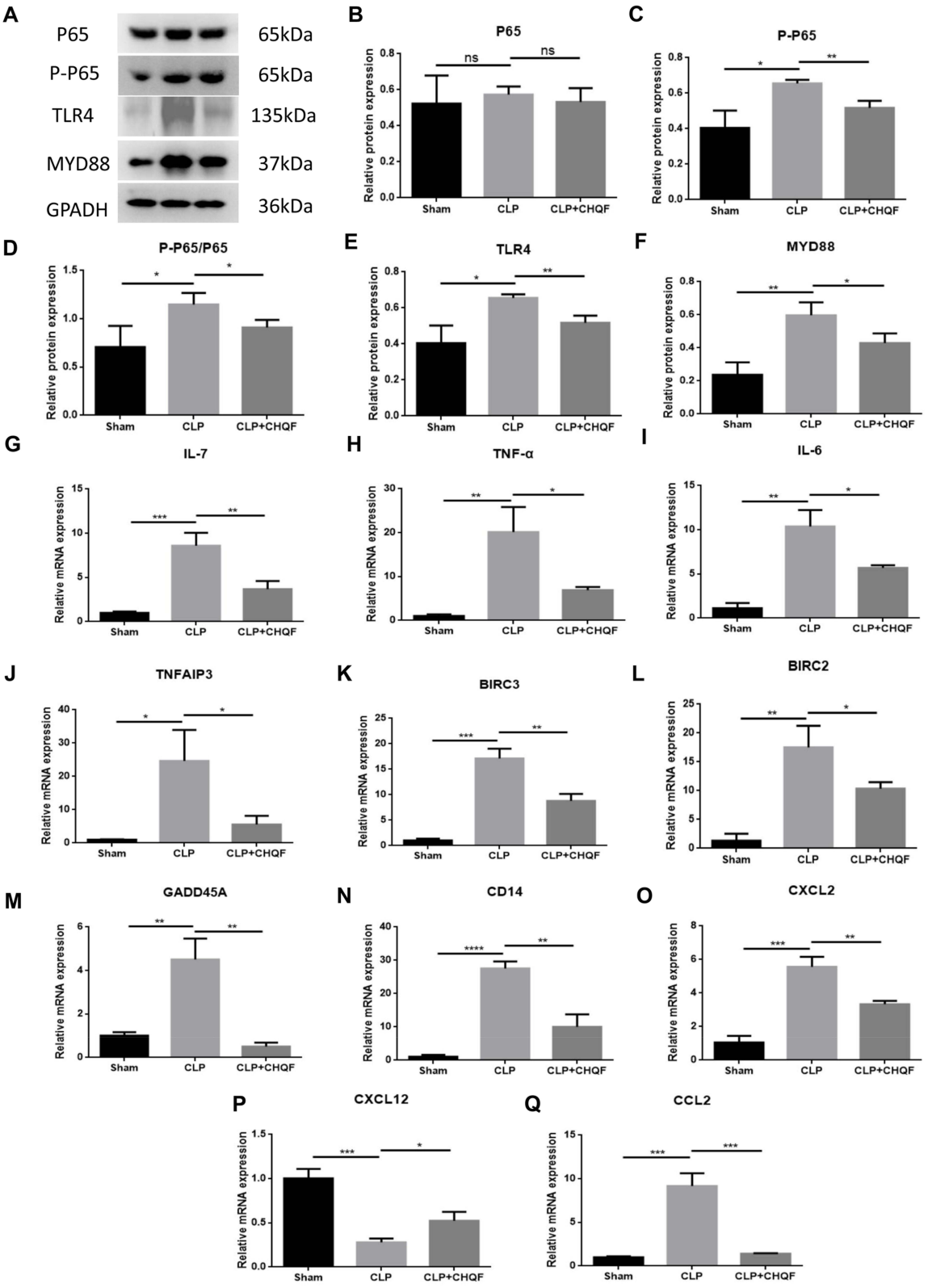

Figure 7 Effects of CHQF on key gene expression and NF-κB pathway proteins in CLP-induced sepsis. (**A**) CHQF inhibits NF-κB signaling in a CLP-induced sepsis mouse model. Protein lysates were subjected to SDS-PAGE followed by immunoblotting for P65, P-P65, TLR4 and MYD88. (**B**–**F**) Statistical analysis for P65, P-P65, P-P65/P65, TLR4 and MYD88 levels. Data are presented as mean ± SD (n = 5 /group). **P* < 0.05, ***P* < 0.01 vs CLP group; ns, not significant. (**G**–**Q**) Detection of IL-7, TNF-α, IL-6, TNFAIP3, BIRC3, BIRC2, GADD45A, CD14, CXCL2, CXCL12, and CCL2 mRNA expression levels in sepsis mice. Data are presented as mean ± SD (n = 5 /group). **P* < 0.05, ***P* < 0.01, ****P* < 0.001, *****P* < 0.0001 vs CLP group; ns, not significant.

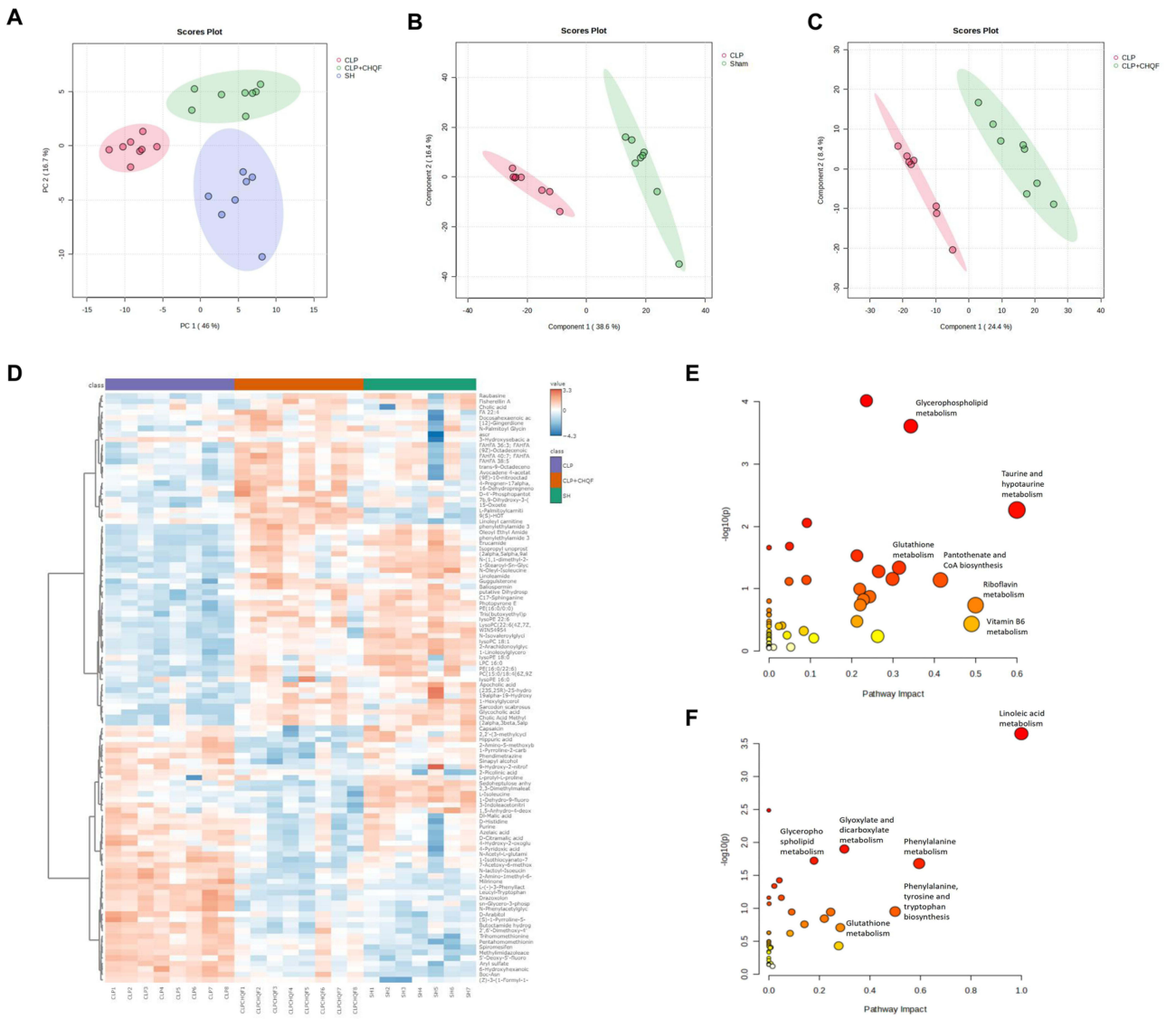

Figure 8 Metabolomics analysis. (**A**) PCA of Sham, CLP, and CLP+CHQF groups. (**B** and **C**) PLS-DA score plot of CLP vs Sham and CLP vs CLP+CHQF. (**D–F**) Metabolic pathways of the significant metabolites in Sham vs CLP and CLP vs CLP+CHQF.(n=8 /group, one data point in the Sham group was identified as an outlier and was excluded from the analysis).

(−7.6 kcal/mol), quercetin-BIRC5 (−7.6 kcal/mol), hyperforin-CXCL8 (−5.5 kcal/mol), wogonin-CXCL8 (−6 kcal/mol), and wogonin-CCL2 (−7 kcal/mol) (Table 6 and Figure 9). All binding energies were ≤ −5 kJ/mol (approximately −1.2 kcal/mol), reflecting strong molecular interactions between these core bioactive compounds and the key target proteins, underscoring their therapeutic potential in sepsis-induced liver injury.

Table 4 Metabolic Pathway Analysis of the Sham Vs CLP Groups

No.	Metabolic Pathway	Total	Hits	FDR	Impact
1	Taurine and hypotaurine metabolism	8	3	0.1458	0.6000
2	Riboflavin metabolism	4	1	0.7748	0.5000
3	Vitamin B6 metabolism	9	1	1.0000	0.4902
4	Pantothenate and CoA biosynthesis	20	3	0.4711	0.4149
5	Glycerophospholipid metabolism	36	8	0.0099	0.3432
6	Glutathione metabolism	28	4	0.4609	0.3147

https://doi.org/10.2147/DDDT.S521626

Table 5 Metabolic Pathway Analysis of the CHQF Vs CLP Groups

No.	Metabolic Pathway	Total	Hits	FDR	Impact
1	Linoleic acid metabolism	5	3	0.0179	1.0000
2	Phenylalanine metabolism	8	2	0.3343	0.5952
3	Phenylalanine, tyrosine and tryptophan biosynthesis	4	1	0.6997	0.5000
4	Glyoxylate and dicarboxylate metabolism	32	4	0.3343	0.2989
5	Glutathione metabolism	28	2	0.9795	0.2829
6	Arachidonic acid metabolism	44	2	1.0000	0.2766

Table 6 Docking Effect Analysis of Compounds and Targets

Compound	Target	PDB ID	Binding Energy (kcal/mol)
Paeoniflorin	CD14	4glp	−6.9
Quercetin	CXCL2	1QNK	−7.8
Quercetin	CCL2	1dok	−7.6
Quercetin	BIRC5	1e31	−7.6
Hyperforin	CXCL8	1IKL	−5.5
Wogonin	CXCL8	1IKL	−6.0
Wogonin	CCL2	1dok	−7.0

Discussion

This study is the first to apply a multi-omics integrative approach to elucidate the mechanisms by which the Chinese herbal medicine CHQF prevents sepsis using a CLP-induced sepsis model. The results indicate that CHQF alleviates sepsis-induced liver injury and regulates the activity of the NF-κB signaling pathway, inflammatory mediators, and their corresponding metabolic products. In this study, we focused on the 24-hour post-CLP period to capture the acute phase of sepsis-induced liver injury, which is characterized by intense inflammatory responses and early organ dysfunction. While this timeframe is widely used and sufficient to evaluate acute therapeutic efficacy, we acknowledge that longer-term observations (eg, 48–72 hours or beyond) could provide additional insights into the sustained effects of CHQF and the progression or resolution of sepsis. Future studies are warranted to explore the chronic phase of sepsis and tissue remodeling.

Sepsis is defined by a dysregulated immune response to infectious insults. Sepsis involves various pathological processes, including pathogen infection, host immune responses, inflammation, and organ dysfunction,[21] which vary among patients, complicating the development of a single drug that is universally effective and affecting multiple aspects of the immune system. Effective immune responses require activation to combat infections and suppression to prevent excessive inflammation and identifying drugs that control infections without exacerbating inflammation is challenging. Consequently, no specific therapies exist for modulating inflammation, immune responses, or oxidative stress. Traditional Chinese medicines (TCM), with their multiple ingredients, can simultaneously target various pathological mechanisms and pathways.[22] This complex mechanism may enable TCM to be effective in the multifaceted pathological processes of sepsis. Compared with single-ingredient western medicines, TCM may be better suited to address the multifactorial causes and progression of sepsis. The CHQF is a modified formulation based on the TCM Qingyin Decoction, which possesses anti-inflammatory, immune-regulating, and organ-protective effects.[23] This study employed a multiomics approach to reveal the therapeutic potential of CHQF for sepsis using a CLP-induced sepsis model. The results demonstrated that CHQF enhances survival rates in septic mice, mitigates sepsis-induced liver injury, reduces the secretion of pro-inflammatory cytokines and chemokines, modulates the NF-κB signaling pathway, and influences associated cytokines and relevant metabolic pathways.

Cytokines are crucial in the inflammatory response; however, they often exhibit bidirectional effects. An appropriate balance between pro-inflammatory and anti-inflammatory cytokines is crucial for effective host defense during sepsis. TNF-α, primarily produced by immune cells activated by infection,[24] stimulates endothelial cells to release additional

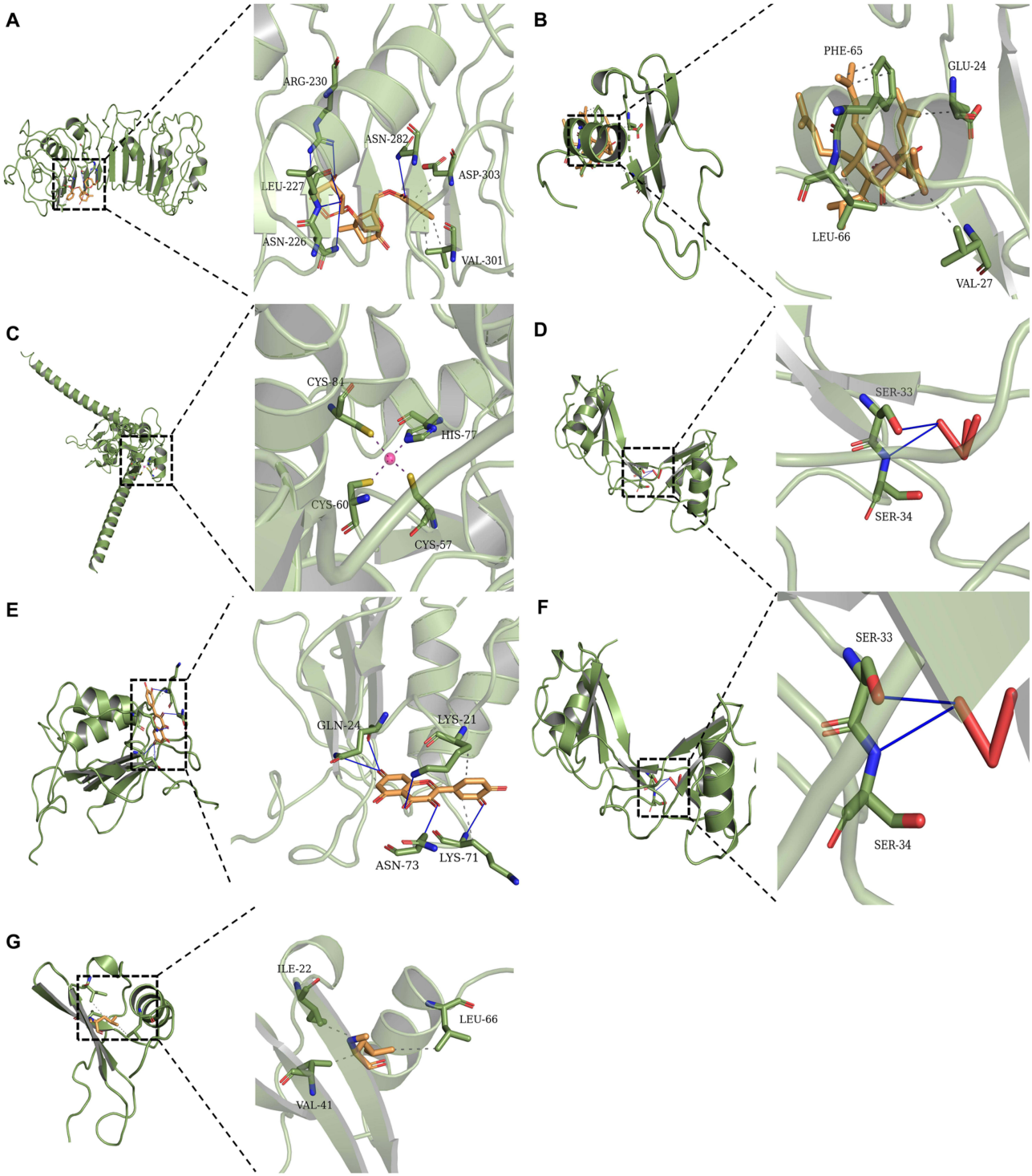

Figure 9 Result of molecular docking. (**A**) CD14-paeoniflorin (−6.9 kcal/mol), (**B**) CXCL8-hyperforin (−7.8 kcal/mol), (**C**) BIRC5-quercetin (−7.6 kcal/mol), (**D**) CCL2-quercetin (−7.6 kcal/mol), (**E**) CXCL2-quercetin (−7.8 kcal/mol), (**F**) CCL2-wogonin (−7.0 kcal/mol), (**G**) CXCL8-wogonin (−6.0 kcal/mol).

inflammatory mediators, increasing vascular permeability and leukocyte migration, thereby promoting and sustaining inflammatory response.[25] Elevated TNF-α levels correlate positively with sepsis severity. IL-6 enhances the inflammatory response by stimulating acute-phase protein synthesis. It is an acute-phase response component in sepsis, with its levels rising significantly in infection and inflammation.[26] In sepsis, IL-6 contributes to the initiation and maintenance of the inflammatory response. Conversely, IL-10, a key anti-inflammatory cytokine, alleviates inflammation by inhibiting pro-

https://doi.org/10.2147/DDDT.S521626

inflammatory cytokine production and suppresses excessive immune activation by reducing immune cell activity, thereby preventing an overreaction of the immune system and subsequent tissue damage.[27] Following CHQF treatment, serum TNF-α and IL-6 levels in mice decreased, while IL-10 levels increased, with significant improvement observed in sepsis-induced liver tissue damage. These findings suggest that the drug possesses anti-inflammatory and immunoregulatory properties, potentially correcting immune dysregulation associated with sepsis and improving clinical outcomes and prognosis.

Network pharmacology integrates various data and methodologies to study drug action mechanisms aiming to elucidate how drugs affect complex biological networks.[28] Molecular docking is a computational approach employed to predict the binding interactions and affinities between small-molecule drug ligands, target macromolecules, and their respective protein receptors.[29] Network pharmacology was employed to elucidate the potential mechanisms of action of CHQF. Sixteen core targets were identified, including TNF, CCL2, IL-6, and AKT. These targets suggest that core compounds and core targets exert their therapeutic effects in sepsis by modulating signaling pathways, including IL-17, TNF, and NF-κB pathways. Molecular docking analysis of key genes identified by RNA-Seq and their corresponding core compounds revealed binding energies between the core targets and their respective core compound ligands, which exhibited binding affinities significantly lower than −5 kJ/mol, indicating robust molecular interactions. The principal bioactive constituents of CHQF include paeoniflorin, quercetin, hyperforin, and wogonin.

Transcriptomics is the scientific study of transcripts and their expression levels in cells or tissue.[30] Using RNA-Seq analyses, we extensively characterized gene expression profiles and functional changes following CHQF administration. CHQF notably reduced the mRNA expression of TNF-α, IL-6, IL-1β, and IL-17, all of which are pivotal in the pathophysiology of sepsis. TNF-α, a key inflammatory mediator, plays a pivotal role in the molecular mechanisms underlying sepsis pathogenesis. It interacts with cell surface receptors, triggering the NF-κB signaling cascade, which promotes inflammatory responses and apoptotic cell death.[31] Excess TNF-α production can lead to oxidative stress, endothelial dysfunction, and increased vascular permeability, causing multi-organ failure.[32] IL-6 is a critical acute-phase protein that modulates immune activation and inflammatory processes by binding to its receptor, activating the JAK/STAT signaling pathway, enhancing the synthesis of acute-phase proteins such as C-reactive protein, and promoting leukocyte production and activation.[33] Elevated IL-6 levels in sepsis indicate the presence of systemic inflammatory response syndrome.[34] IL-1β, a potent pro-inflammatory cytokine, binds to the IL-1 receptor to activate NF-κB and MAPK signaling pathways, which upregulate the synthesis of pro-inflammatory mediators.[35] In sepsis, IL-1β induces inflammation and apoptosis, increases endothelial permeability, and contributes to vascular damage and tissue edema.[36] IL-17, produced by Th17 cells, is a pro-inflammatory mediator that plays a key role in modulating immune and inflammatory pathways.[37] It interacts with the IL-17 receptor, triggering downstream NF-κB and MAPK signaling pathways, thus promoting the release of additional pro-inflammatory cytokines, including IL-6 and IL-8.[38] In sepsis, IL-17 may enhance local and systemic inflammatory responses by recruiting and activating inflammatory cells.[39] Our study indicated that these cytokines were significantly elevated in mice with CLP-induced sepsis, but their expression was markedly suppressed post-CHQF treatment. These results suggested that CHQF alleviates sepsis-induced inflammatory infections by modulating these proinflammatory cytokine levels.

Additionally, CHQF modulates chemokine expression, including CCL2, CCL3, CCL4, CXCL2, CXCL3, and CXCL5. CCL2 plays a crucial role in recruiting and activating monocytes, T cells, and immature dendritic cells, thereby triggering localized inflammatory responses, mainly through its interaction with the receptor CCR2.[40] This interaction promotes chemotaxis in monocytes, macrophages, and dendritic cells.[41] In sepsis, the increased CCL2 expression facilitates immune cell recruitment to the infection site, enhancing local inflammatory responses.[42] CCL3, by binding to its receptors CCR1 and CCR5, facilitates the chemotaxis of monocytes and T cells. It also regulates immune cell recruitment and inflammatory responses in sepsis.[43] CCL4 primarily regulates immune cell migration via the CCR5 receptor. In sepsis, CCL4 promotes the recruitment of monocytes, T, and natural killer cells, contributing to inflammatory response and immune modulation.[44] CXCL2 promotes chemotaxis and neutrophil activation by binding to its receptor, CXCR2.[45] Enhancing local immune responses through neutrophil recruitment is crucial in sepsis. Similarly, CXCL5 and CXCL3 bind to CXCR2 to promote chemotaxis and neutrophil activation. They contribute to the recruitment of neutrophils and the regulation of inflammatory responses in sepsis.[46] In mice with sepsis, these chemokines were significantly upregulated; however, their levels were

markedly downregulated following CHQF treatment. The reduction in inflammatory cell infiltration observed following CHQF treatment may be attributed to the suppression of these chemokines.

A comprehensive metabolomic analysis demonstrated that Chaihuang Qingfu (CHQF) exerts significant regulatory effects on key metabolic pathways implicated in sepsis. These include the upregulation of linoleic acid and arachidonic acid metabolism, along with the downregulation of glyoxylate and glutathione metabolism. Linoleic acid metabolism plays a pivotal role in modulating the inflammatory response in sepsis, primarily through the biosynthesis of anti-inflammatory eicosanoids such as epoxyeicosatrienoic acids (EETs), which exert both anti-inflammatory and vasoprotective effects. The observed upregulation of this pathway following CHQF administration suggests that it may facilitate the synthesis of anti-inflammatory lipid mediators, thereby attenuating the systemic inflammatory response characteristic of sepsis. In the context of arachidonic acid metabolism, excessive activation of this pathway promotes the overproduction of pro-inflammatory eicosanoids, including leukotrienes and prostaglandins, which exacerbate the inflammatory cascade in sepsis.[47] CHQF appears to modulate this pathway by suppressing the release of pro-inflammatory mediators while enhancing the synthesis of anti-inflammatory lipoxins, potentially contributing to improved sepsis outcomes. Additionally, the downregulation of glutathione metabolism observed following CHQF treatment suggests a reduction in oxidative stress.[48] Sepsis is frequently associated with glutathione depletion, which compromises the cellular redox balance and promotes oxidative damage. CHQF may exert a protective effect by decreasing reactive oxygen species (ROS) generation, thereby alleviating oxidative stress and reducing the cellular demand for glutathione. The downregulation of glycerophospholipid metabolism further highlights the potential of CHQF in restoring cell membrane integrity.[49] Metabolomic profiling identified excessive activation of phospholipase A2 (PLA2) in sepsis, leading to the accumulation of lysophospholipids, such as lysophosphatidylcholines (LysoPCs), which disrupt membrane stability and amplify inflammatory responses.[50] CHQF may counteract these pathological changes by inhibiting PLA2 activity, thereby reducing membrane phospholipid degradation and mitigating membrane-associated damage. 2-Arachidonoylglycerol (2-AG), an endogenous cannabinoid with immunomodulatory and anti-inflammatory properties,[51] is markedly reduced in sepsis, leading to excessive immune activation and heightened inflammatory responses. CHQF may exert its therapeutic effects by restoring 2-AG levels, thereby tempering immune hyperactivation and alleviating sepsis-induced inflammation. LysoPCs are recognized as biomarkers of inflammation, with their biological effects being contingent on both concentration and microenvironmental context.[52] At low concentrations, LysoPC 18:1 has been shown to activate peroxisome proliferator-activated receptor gamma (PPARγ), leading to the suppression of nuclear factor kappa B (NF-κB) signaling and subsequent attenuation of the inflammatory response.[53] CHQF may restore LysoPC 18:1 to homeostatic levels, thereby modulating the balance between pro-inflammatory and anti-inflammatory signaling to mitigate inflammation in sepsis. Furthermore, itaconate, a metabolite synthesized in macrophages via immune-responsive gene 1 (Irg1), serves as a critical marker of inflammation and oxidative stress.[54] Its accumulation inhibits succinate dehydrogenase (SDH), thereby exacerbating mitochondrial dysfunction and promoting excessive immune cell activation.[55] The observed reduction in itaconate levels following CHQF treatment suggests that CHQF may exert a protective effect by modulating Irg1 expression or suppressing macrophage hyperactivation, ultimately mitigating sepsis-associated mitochondrial oxidative damage.

Given the complexity and heterogeneity of sepsis, current therapeutic strategies remain largely supportive and nonspecific. Our integrated omics analysis reveals the multi-target nature of CHQF, suggesting its potential as a promising adjunctive therapy for sepsis-induced liver injury. CHQF's ability to modulate key inflammatory pathways, such as NF-κB, and restore metabolic homeostasis highlights its potential for clinical translation. Moreover, based on our comprehensive analysis, CHQF demonstrates significant pharmacological effects on these targets. However, the precise mechanisms underlying these internal interactions have yet to be fully elucidated, warranting further investigation. To validate its safety and efficacy in humans, additional studies, including pharmacokinetic profiling, toxicity evaluation, and clinical trials, are essential.

Conclusion

In conclusion, this research evaluated CHQF's efficacy in addressing sepsis and explored its molecular mechanisms of action. By integrating network pharmacology, transcriptomics, metabolomics, and experimental validations, we

demonstrated that CHQF alleviates CLP-induced sepsis-related liver damage by modulating the NF-κB signaling pathway, associated metabolites, and cytokine expression. Given the complexity of TCM and its multi-target and multi-component nature, further research is needed to validate the identified potential targets. This study reveals novel mechanisms by which CHQF mitigates sepsis-induced liver injury, highlighting its potential therapeutic capabilities.

Acknowledgments

This work was supported by Hunan Provincial Natural Science Foundation Key projects of Hunan Provincial Administration of Traditional Chinese Medicine (A2024040), Hunan Province Natural Science Foundation (2024JJ8145).

Disclosure

The authors declare no competing financial interest.

References

1. Oczkowski S, Alshamsi F, Belley-Cote E, et al. Surviving sepsis campaign guidelines 2021: highlights for the practicing clinician. *Pol Arch Intern Med*. 2022;132:7–8. doi:10.20452/pamw.16290
2. Weng L, Xu Y, Yin P, et al. National incidence and mortality of hospitalized sepsis in China. *Crit Care*. 2023;27(1):84. doi:10.1186/s13054-023-04385-x
3. Liu D, Huang SY, Sun JH, et al. Sepsis-induced immunosuppression: mechanisms, diagnosis and current treatment options. *Mil Med Res*. 2022;9(1):56. doi:10.1186/s40779-022-00422-y
4. Nedeva C. Inflammation and cell death of the innate and adaptive immune system during sepsis. *Biomolecules*. 2021;11(7):1011. doi:10.3390/biom11071011
5. Wang Z, Liu J, Li F, et al. Mechanisms of Qingyi decoction in severe acute pancreatitis-associated acute lung injury via gut microbiota: targeting the short-chain fatty acids-mediated AMPK/NF-kappaB/NLRP3 pathway. *Microbiol Spectr*. 2023;11(4):e0366422. doi:10.1128/spectrum.03664-22
6. Li L, Li YQ, Sun ZW, et al. Qingyi decoction protects against myocardial injuries induced by severe acute pancreatitis. *World J Gastroenterol*. 2020;26(12):1317–1328. doi:10.3748/wjg.v26.i12.1317
7. Zhang P, Zhang D, Zhou W, et al. Network pharmacology: towards the artificial intelligence-based precision traditional Chinese medicine. *Brief Bioinform*. 2023;25(1):1. doi:10.1093/bib/bbad518
8. Hu L, Liu J, Zhang W, et al. Functional metabolomics decipher biochemical functions and associated mechanisms underlie small-molecule metabolism. *Mass Spectrom Rev*. 2020;39(5–6):417–433. doi:10.1002/mas.21611
9. Chen Q, Liang X, Wu T, et al. Integrative analysis of metabolomics and proteomics reveals amino acid metabolism disorder in sepsis. *J Transl Med*. 2022;20(1):123. doi:10.1186/s12967-022-03320-y
10. Liu J, Zhang Q, Wong YK, et al. Single-cell transcriptomics reveals the ameliorative effect of oridonin on septic liver injury. *Adv Biol*. 2024;8(3):e2300542. doi:10.1002/adbi.202300542
11. Dai W, Zheng P, Wu J, et al. Integrated analysis of single-cell RNA-seq and chipset data unravels PANoptosis-related genes in sepsis. *Front Immunol*. 2023;14:1247131. doi:10.3389/fimmu.2023.1247131
12. Yang S, Guo J, Kong Z, et al. Causal effects of gut microbiota on sepsis and sepsis-related death: insights from genome-wide Mendelian randomization, single-cell RNA, bulk RNA sequencing, and network pharmacology. *J Transl Med*. 2024;22(1):10. doi:10.1186/s12967-023-04835-8
13. Cheng PL, Chen HH, Jiang YH, et al. Using RNA-Seq to investigate immune-metabolism features in immunocompromised patients with sepsis. *Front Med Lausanne*. 2021;8:747263. doi:10.3389/fmed.2021.747263
14. Jin GL, Liu HP, Huang YX, et al. Koumine regulates macrophage M1/M2 polarization via TSPO, alleviating sepsis-associated liver injury in mice. *Phytomedicine*. 2022;107:154484. doi:10.1016/j.phymed.2022.154484
15. Yang Y, Chen Q, Fan S, et al. Glutamine sustains energy metabolism and alleviates liver injury in burn sepsis by promoting the assembly of mitochondrial HSP60-HSP10 complex via SIRT4 dependent protein deacetylation. *Redox Rep*. 2024;29(1):2312320. doi:10.1080/13510002.2024.2312320
16. Zheng G, Pan M, Jin W, Jin G, Huang Y. MicroRNA-135a is up-regulated and aggravates myocardial depression in sepsis via regulating p38 MAPK/NF-kappaB pathway. *Int Immunopharmacol*. 2017;45:6–12. doi:10.1016/j.intimp.2017.01.029
17. Xiao W, Shi H, Tian Y, Chen F, Han X, Jiang Y. Chaihuang Qingfu pills protect against acute pancreatitis-associated acute lung injury through MMP9-NLRP3-pyroptosis pathway. *J Inflamm Res*. 2025;18:2317–2338. doi:10.2147/JIR.S501531
18. Ishak K, Baptista A, Bianchi L, et al. Histological grading and staging of chronic hepatitis. *J Hepatol*. 1995;22(6):696–699. doi:10.1016/0168-8278(95)80226-6
19. Hu X, Qi C, Feng F, et al. Combining network pharmacology, RNA-seq, and metabolomics strategies to reveal the mechanism of cimicifugae rhizoma - smilax glabra roxb herb pair for the treatment of psoriasis. *Phytomedicine*. 2022;105:154384. doi:10.1016/j.phymed.2022.154384
20. Chen T, Wang T, Shi Y, et al. Integrated network pharmacology, metabolomics and molecular docking analysis to reveal the mechanisms of quercetin in the treatment of hyperlipidemia. *J Pharm Biomed Anal*. 2025;252:116507. doi:10.1016/j.jpba.2024.116507
21. Wang W, Liu CF. Sepsis heterogeneity. *World J Pediatr*. 2023;19(10):919–927. doi:10.1007/s12519-023-00689-8
22. Singer M, Deutschman CS, Seymour CW, et al. The third international consensus definitions for sepsis and septic shock (Sepsis-3). *JAMA*. 2016;315(8):801–810. doi:10.1001/jama.2016.0287

23. Fan X, Mai C, Zuo L, et al. Herbal formula BaWeiBaiDuSan alleviates polymicrobial sepsis-induced liver injury via increasing the gut microbiota lactobacillus johnsonii and regulating macrophage anti-inflammatory activity in mice. *Acta Pharm Sin B*. 2023;13(3):1164–1179. doi:10.1016/j.apsb.2022.10.016
24. Deng P, Tang N, Li L, Zou G, Xu Y, Liu Z. Diagnostic value of combined detection of IL-1beta, IL-6, and TNF-alpha for sepsis-induced cardiomyopathy. *Med Clin*. 2022;158(9):413–417. doi:10.1016/j.medcli.2021.04.025
25. Liu A, Xun S, Zhou G, Zhang Y, Lin L. Honokiol alleviates sepsis-associated cardiac dysfunction via attenuating inflammation, apoptosis and oxidative stress. *J Pharm Pharmacol*. 2023;75(3):397–406. doi:10.1093/jpp/rgac102
26. Liu S, Xie J, Duan C, et al. ADAR1 inhibits macrophage apoptosis and alleviates sepsis-induced liver injury through miR-122/BCL2A1 signaling. *J Clin Transl Hepatol*. 2024;12(2):134–150. doi:10.14218/JCTH.2023.00171
27. York AG, Skadow MH, Oh J, et al. IL-10 constrains sphingolipid metabolism to limit inflammation. *Nature*. 2024;627(8004):628–635. doi:10.1038/s41586-024-07098-5
28. Wang T, Li S, Wu Y, et al. Mechanistic investigation of Xuebijing for treatment of paraquat-induced pulmonary fibrosis by metabolomics and network pharmacology. *ACS Omega*. 2021;6(30):19717–19730. doi:10.1021/acsomega.1c02370
29. Jia X, Gu M, Dai J, Wang J, Zhang Y, Pang Z. Quercetin attenuates Pseudomonas aeruginosa-induced acute lung inflammation by inhibiting PI3K/AKT/NF-kappaB signaling pathway. *Inflammopharmacology*. 2024;32(2):1059–1076. doi:10.1007/s10787-023-01416-5
30. Withanage MHH, Liang H, Zeng E. RNA-Seq experiment and data analysis. *Methods Mol Biol*. 2022;2418:405–424. doi:10.1007/978-1-0716-1920-9_22
31. Tiegs G, Horst AK. TNF in the liver: targeting a central player in inflammation. *Semin Immunopathol*. 2022;44(4):445–459. doi:10.1007/s00281-022-00910-2
32. Wang T, He C. TNF-alpha and IL-6: the link between immune and bone system. *Curr Drug Targets*. 2020;21(3):213–227. doi:10.2174/1389450120666190821161259
33. Kaur S, Bansal Y, Kumar R, Bansal G. A panoramic review of IL-6: structure, pathophysiological roles and inhibitors. *Bioorg Med Chem*. 2020;28(5):115327. doi:10.1016/j.bmc.2020.115327
34. Zhou J, Li S, Zeng Z. Dendrobine alleviates LPS-induced acute lung injury via activation of the PI3K/AKT/GSK3beta pathway. *J Ethnopharmacol*. 2025;346:119634. doi:10.1016/j.jep.2025.119634
35. Busch K, Kny M, Huang N, et al. Inhibition of the NLRP3/IL-1beta axis protects against sepsis-induced cardiomyopathy. *J Cachexia, Sarcopenia Muscle*. 2021;12(6):1653–1668. doi:10.1002/jcsm.12763
36. Xiong S, Hong Z, Huang LS, et al. IL-1beta suppression of VE-cadherin transcription underlies sepsis-induced inflammatory lung injury. *J Clin Invest*. 2020;130(7):3684–3698. doi:10.1172/JCI136908
37. Huangfu L, Li R, Huang Y, Wang S. The IL-17 family in diseases: from bench to bedside. *Signal Transduct Target Ther*. 2023;8(1):402. doi:10.1038/s41392-023-01620-3
38. Schinocca C, Rizzo C, Fasano S, et al. Role of the IL-23/IL-17 pathway in rheumatic diseases: an overview. *Front Immunol*. 2021;12:637829. doi:10.3389/fimmu.2021.637829
39. Ghoreschi K, Balato A, Enerback C, Sabat R. Therapeutics targeting the IL-23 and IL-17 pathway in psoriasis. *Lancet*. 2021;397(10275):754–766. doi:10.1016/S0140-6736(21)00184-7
40. Cui TX, Brady AE, Fulton CT, et al. CCR2 mediates chronic LPS-induced pulmonary inflammation and hypoalveolarization in a murine model of bronchopulmonary dysplasia. *Front Immunol*. 2020;11:579628. doi:10.3389/fimmu.2020.579628
41. Yang H, Zhang Q, Xu M, et al. CCL2-CCR2 axis recruits tumor associated macrophages to induce immune evasion through PD-1 signaling in esophageal carcinogenesis. *Mol Cancer*. 2020;19(1):41. doi:10.1186/s12943-020-01165-x
42. Gomes RN, Teixeira-Cunha MG, Figueiredo RT, et al. Bacterial clearance in septic mice is modulated by MCP-1/CCL2 and nitric oxide. *Shock*. 2013;39(1):63–69. doi:10.1097/SHK.0b013e31827802b5
43. Sheng D, Ma W, Zhang R, et al. Ccl3 enhances docetaxel chemosensitivity in breast cancer by triggering proinflammatory macrophage polarization. *J Immunother Cancer*. 2022;10(5):5. doi:10.1136/jitc-2021-003793
44. Wu BM, Liu JD, Li YH, Li J. Margatoxin mitigates CCl4-induced hepatic fibrosis in mice via macrophage polarization, cytokine secretion and STAT signaling. *Int J Mol Med*. 2020;45(1):103–114. doi:10.3892/ijmm.2019.4395
45. Wang T, Zhou Y, Zhou Z, et al. Secreted protease PRSS35 suppresses hepatocellular carcinoma by disabling CXCL2-mediated neutrophil extracellular traps. *Nat Commun*. 2023;14(1):1513. doi:10.1038/s41467-023-37227-z
46. Korbecki J, Kojder K, Kapczuk P, et al. The effect of hypoxia on the expression of CXC chemokines and CXC chemokine receptors-A review of literature. *Int J Mol Sci*. 2021;22(2). doi:10.3390/ijms22020843
47. Bottoms GD, Adams HR. Involvement of prostaglandins and leukotrienes in the pathogenesis of endotoxemia and sepsis. *J Am Vet Med Assoc*. 1992;200(12):1842–1848. doi:10.2460/javma.1992.200.12.1842
48. Wang C, Yuan W, Hu A, et al. Dexmedetomidine alleviated sepsis-induced myocardial ferroptosis and septic heart injury. *Mol Med Rep*. 2020;22(1):175–184. doi:10.3892/mmr.2020.11114
49. Huang J, Wang Z, Zhang X, et al. Lipidomics study of sepsis-induced liver and lung injury under Anti-HMGB1 intervention. *J Proteome Res*. 2023;22(6):1881–1895. doi:10.1021/acs.jproteome.2c00851
50. Feng S, Cui N, Zhao W, et al. Prognostic biomarkers for sepsis mortality based on the literature and LC-MS-based metabolomics of sepsis patients. *Am J Transl Res*. 2023;15(9):5757–5768.
51. Kayganich-Harrison KA, Murphy RC. Characterization of chain-shortened oxidized glycerophosphocholine lipids using fast atom bombardment and tandem mass spectrometry. *Anal Biochem*. 1994;221(1):16–24. doi:10.1006/abio.1994.1372
52. Lasky-Su J, Dahlin A, Litonjua AA, et al. Metabolome alterations in severe critical illness and vitamin D status. *Crit Care*. 2017;21(1):193. doi:10.1186/s13054-017-1794-y
53. Li X, Yin Z, Yan W, et al. Association between changes in plasma metabolism and clinical outcomes of sepsis. *Emerg Med Int*. 2023;2023:2590115. doi:10.1155/2023/2590115
54. He R, Liu B, Xiong R, et al. Itaconate inhibits ferroptosis of macrophage via Nrf2 pathways against sepsis-induced acute lung injury. *Cell Death Discov*. 2022;8(1):43. doi:10.1038/s41420-021-00807-3
55. Xu L, Cai J, Li C, et al. 4-Octyl itaconate attenuates LPS-induced acute kidney injury by activating Nrf2 and inhibiting STAT3 signaling. *Mol Med*. 2023;29(1):58. doi:10.1186/s10020-023-00631-8